Machine learning for assessing variability of the long-term projections of the hydropower generation on a European scale

Valentina Sessa, Edi Assoumou, Mireille Bossy, Sílvia Carvalho, Sofia Simoes

Machine learning for assessing variability of the long-term projections of the hydropower generation on a European scale

Valentina Sessa[1], Edi Assoumou[1], Mireille Bossy[11], Sílvia Carvalho[2], and Sofia G. Simoes[3]

[1]MINES ParisTech, Centre de Mathématiques Appliquées (CMA), Sophia Antipolis, France.
[11]Université Côte d'Azur, Inria, France.
[2]CCIAM, Centre for Ecology, Evolution and Environmental Changes (cE3c), Faculty of Sciences of the University of Lisbon, Portugal.
[3]CENSE Center for Enviroment and Sustainability Research, NOVA School for SCIENCE and Technology, NOVA University Lisbon, Caparica, Portugal.

March 13, 2020

Abstract

A big challenge of sustainable power systems is the integration of climate variability into the operational and long-term planning processes. In this paper, we focus on the run-of-river based hydropower generation on a European scale. In particular, we deal with the modeling of this form of power production based on climate variables. Translating time series of climate data (precipitation and air temperature) into time series of run-of-river based hydropower generation is not an easy task as it is necessary to capture the complex relationship between the availability of water and the generation of electricity. Indeed, this kind of electricity generation is limited by the flow of the river in which the power plants are located. Moreover, the water flow is a nonlinear function of the climate variables and the geographical characteristics of the river basins. Finally, the impact of the climate variables on the runoff may occur with a certain delay, whose determination depends on physically based phenomena (e.g., melting snow–local temperature). In this work, we first compare well-established machine learning regression algorithms to be used for modeling the run-of-river hydropower generation. Then, the technique showing to have the best performance is used for producing long-term estimates of hydropower capacity factors based on future climate scenarios for each European country.

Keywords: Energy modeling; machine learning; hydropower generation; energy and climate systems.

1 Introduction

Hydropower (HP) is the world's most dominant (86%) source of renewable electrical energy [1]. Installed hydropower capacity continues to grow quickly with the aim at empowering the transition towards climate neutrality. This is in line with the long-term objectives of the European Community strategy, which called for fully decarbonized power generation by 2050. This means that more than 80% of the EU's electricity will be produced by renewable energy sources. During 2018, more than 21.8 GW of renewable hydroelectric capacity was put into operation worldwide (2.2 GW in Europe) [1].

Table 1: Top five EU countries by installed hydropower capacity (2019) (*excluding pumping storage).

Country	**Total Installed Capacitity(*) (RoR + Res)** [MW]	**Total Generated** [TWh]
Norway	28675 (992 + 27683)	139.51
Spain	20302 (1156 + 19146)	34.12
France	19234 (10955 + 8279)	63.10
Italy	14507 (10650 + 3857)	49.28
Austria	7998 (5558 + 2440)	16.29

Hydropower is either produced in run-of-river (RoR) plants with low hydraulic heads or from water stored in accumulation lakes with hydraulic heads up to several hundred meters (Res), possibly with recirculation of water between lower and higher level reservoirs in so-called pump-storage systems. Among these existing technologies, we focus on the run-of-river based one, which is the most affected by climate. This exists alongside rivers and does not contain large reservoir to store or regulate the flow of the adjacent river. Typically, it generates electricity according to the water flow. This latter is defined by seasonal patterns of precipitation, evaporation, drainage, and other characteristics, which all depend on the geography and climate peculiarity of locations [2]. Although the seasonal patterns of wet and dry seasons are relatively predictable, they are not guaranteed and can change from one year to another [3]. An assessment of climate change impacts on hydroelectric generation in different climate regions requires an in-depth analysis of individual case studies. Given the dominance of local conditions, generalizations are difficult, sometimes even for small regions. Another difficulty is the determination of the temporal relation between the hydropower generation and climate variables. In fact, the impact of the climate variables on the water flow, and on the corresponding power production, may occur with a certain delay, whose determination depends on physically based phenomena. For instance, the melting process of snow at high altitude requires a certain amount of time which depends on the local air temperature. Therefore, the increment of the water flow due to the snow fallen during the winter period may occur only after many months with an increase of the temperature. Due to climate changes, such delay is not easy to be predicted.

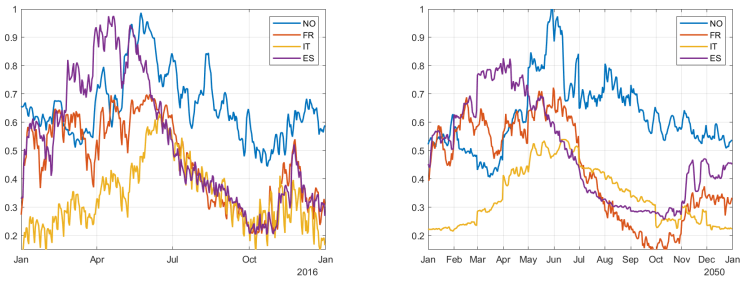

(a) 2016 (b) 2050

Figure 1: Capacity factor of the run-of-river hydropower generation over 2016 (Source: ENTSO-E), and simulated values over 2050 under one of the climate scenarios (A85) for four European countries.

An overview on the run-of-river HP generation of some European countries for the years 2016 and 2050 is shown in Figure 1. In these figures, we can observe the daily variation of the hydropower capacity factor and its variation along the years. For instance, note a decrease of about 10% in the capacity factor for Spain in the spring period of 2050. Indeed, as our results will show, Western South and central Europe are expected to have a decrease in the annual average RoR hydropower production at the target years 2030 and 2050. It is also worthy to note the quite different shapes of the capacity factors for these four countries. This happens even with the values belonging to Spain and Italy, which are countries with similar climate (Mediterranean climate). More details about the projections of climate data and of hydropower production are provided in the next sections.

By what discussed so far, it is clear that the definition of a common hydrological model for all European countries subject to different climate conditions is not an easy task. In this paper, we use Machine Learning (ML) techniques which have the advantage of catching specific trends and patterns in large volumes of data. The obtained models along with the projection of climate data are then used for the prediction of the daily national HP generation in terms of capacity factor (i.e., fraction of produced power over the installed one) for all European countries.

In the literature, it has been shown that machine learning methods are well-suited to the domain of wind speed and wind power prediction [4] and also for solar radiation and solar production [5]. ML techniques have also been applied for the run-off forecast, see [6] and references therein, but at the best of our knowledge few attention has been dedicated in the literature to the prediction of run-of-river hydropower generation from climate data. The reason for this lack could be due to the fact that, while the spatial-temporal relation between wind speed-wind power generation (solar radiation-solar power) is local [7], the one between climate variables, river run-off and hydropower generation is way more complex, as we explained above.

It is also interesting to look at the percentages of hydro, wind and solar power share of the electric power produced in 2018. For instance, in France, we have 12.5%, 5.1%, and 1.9%, respectively (it was $10.1\%, 4.5\%,$ and 1.7% in 2017; Source: RTE), in Portugal it is 25.7%, 24.3% and 1.6%, respectively, (it was

$12.8\%, 20.6\%$, and 1.7% in 2017; Source: REN), finally, in Spain we have 13.5%, 19.8% and 4.6% ($7.5\%, 19\%$, and 3.2% in 2017; Source: REE). As highlighted by these data, differently from wind and solar production, there exists a high variability of hydropower generation from a year to another. This behavior, which is mainly due to climate impact, makes the prediction very challenging, but decisive for the optimal power planning [8, 9].

The recent paper [10] also applies machine learning for the modeling of hydropower production based on climate data but with a completely different goal. Indeed, the machine learning output is used to create hydropower hindcasts to investigate the relationship between the North Atlantic Oscillation and climate variables. Their analysis is focused on the past period 1979-2017, while in this paper we use the best performing ML models for predicting the hydroelectricity generation for the target years 2030 and 2050.

This work is carried on within the CLIM2POWER project [11], whose overall goal is to provide improved guidance to power systems' stakeholders by combining high resolution climate variables and enhanced energy system model. The values of hydropower production computed in this paper will be then used as input for stochastic versions of energy system models for assessing the impact of the climate variability on the optimal operation of the EU power system. A first attempt of a fully integrated analysis of climate impact on the European power system is given in [12]. Some studies on the impact of climate change on hydro-dominated power systems can be found in [13]-[14] for South America, in [15] for Asia, in [16] Africa and, finally, in [17] for U.S.

The paper is organized as follows. In Section 3, we present the historical energy and climate data and we describe how the climate projections are provided. Section 3 includes a brief description of the ML algorithms and the evaluation criteria used in this paper. We dedicate Section 4 to the presentation of the main results. Section 5 concludes this paper providing final remarks and future research ideas.

2 Materials

2.1 Historical data

Climate data include the daily time series of precipitation (TP) and air temperature (AT) remapped to the 6 km COSMO-REA grid. Reanalysis climate data covering the period 1995-2019 are provided by one of the Clim2Power partners, that is Deutscher Wetterdienst (DWD) [18].

Historical data of hydropower production aggregated at country level are from the ENTSO-E Transparency Platform [19], where energy demand and generation data are systematically collected at hourly time resolution starting from 1 January 2015 to the current days. Although this period is relatively short, we will show that our models are able to reproduce the climate impact on run-of-river hydroelectricity production, although some extreme events are still difficult to be predicted. Nevertheless, we are confident that the validity of our approach still holds and it will improve with the increase of historical data.

2.2 Climate projections

In order to obtain climate projections, eleven combinations of Regional Climate Models (RCM) and their driving Global Climate Models (GCMs) were selected (Table 2) from the extensive database provided by the World Climate Research Programme's CORDEX initiative. Datasets are freely available through the Earth System Grid Federation (ESGF) Nodes, and more information on the CORDEX framework can be found in, e.g [20, 21]. Considering a single RCM-GCM combination would imply analyzing only one of a large range of possible outcomes. Instead, the use of several models guarantees a 'better' estimation, as a high level of uncertainty performed by individual models is expected. Moreover, the accuracy of a scenario is defined by both the RCM and its driving GCM. Averaging climate model outputs is commonly done, yet the average might mask the results and smooth the heterogeneity in climate change regimes.

The simulations cover the European domain (EURO-CORDEX), and the spatial resolution considered for this study was the highest available, i.e., 0.11 (around 12.5 km) (EUR-11). For each climate variable, i.e., precipitation and air temperature, daily time series were provided. Special attention needs to be paid when analyzing the state of the climate system for short time periods. In this context, simulations were provided along the twenty-first century focusing on near-future and mid-century (20 years long centered at 2030 and 2050, respectively).

Table 2: List of climate models generating the climate projections and scenarios.

Regional Climate Model (RMC)	**Driving Global Climate Model (GCM)**	**Short code**
CLMcom-CCLM4-8-17	CNRM-CERFACS-CNRM-CM5	A45 - A85
CLMcom-CCLM4-8-17	ICHEC-EC-EARTH	B45 - B85
SMHI-RCA4	ICHEC-EC-EARTH	C45 - C85
DMI-HIRHAM5	ICHEC-EC-EARTH	D45 - D85
KNMI-RACMO22E	ICHEC-EC-EARTH	E45 - E85
IPSL-INERIS-WRF331F	IPSL-IPSL-CM5A-MR	F45 - F85
SMHI-RCA4	IPSL-IPSL-CM5A-MR	G45 - G85
KNMI-RACMO22E	MOHC-HadGEM2-ES	H45 - H85
SMHI-RCA4	MOHC-HadGEM2-ES	I45 - I85
MPI-CSC-REMO2009	MPI-M-MPI-ESM-LR	J45 - J85
DMI-HIRHAM5	NCC-NorESM1-M	L45 - L85

Regarding the main sources of uncertainty of climate projections, apart from the ones already mentioned, such as the uncertainty inherent in the model by itself, and the internal natural variability, the uncertainty of the climate scenarios is also considered. Data comprises future projections under two different Representative Concentration Pathways (RCPs 4.5 and 8.5), which are scenarios that include time series of emissions and concentrations of the full suite of greenhouse gases and aerosols and chemically active gases, as well as land use. The RCP4.5 is an intermediate stabilization pathway in which radiative forcing is stabilized at approximately 4.5 W/m^2, while for RCP8.5 the radiative forcing reaches greater than 8.5 W/m^2 by 2100 and continues to rise for some amount of time [22].

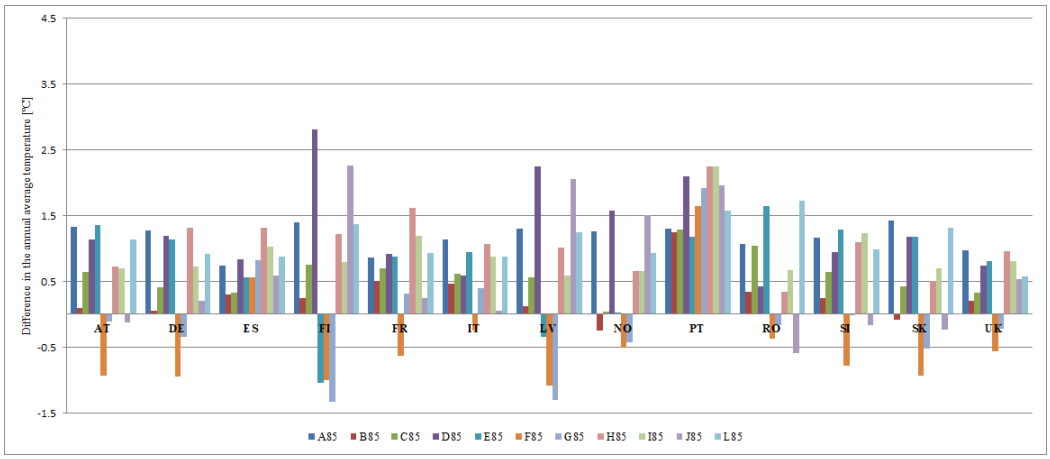

(a) 2030

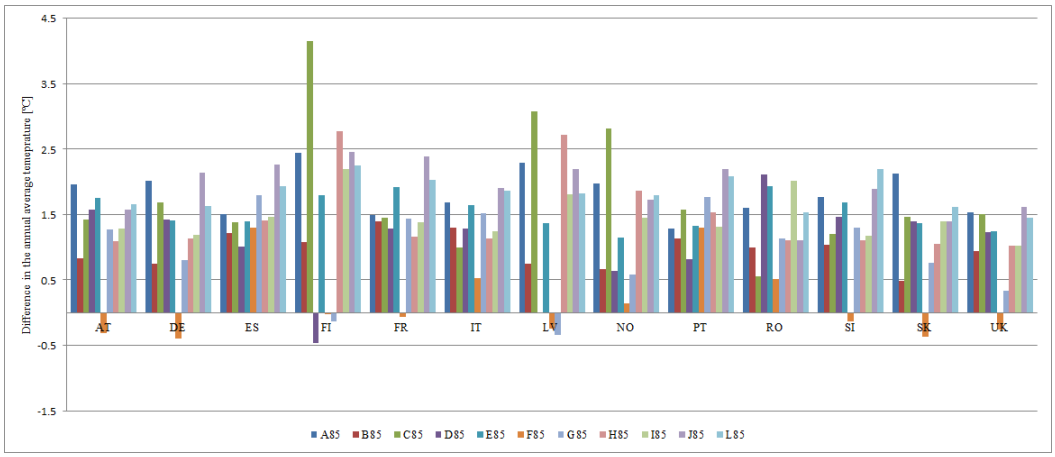

(b) 2050

Figure 2: Difference in the annual average temperature per country: comparison 2016 and projections for 2030 and 2050 under RCP 8.5.

The output of the climate projection models are adjusted with respected to the reanalysis data for the year 2016 [23].

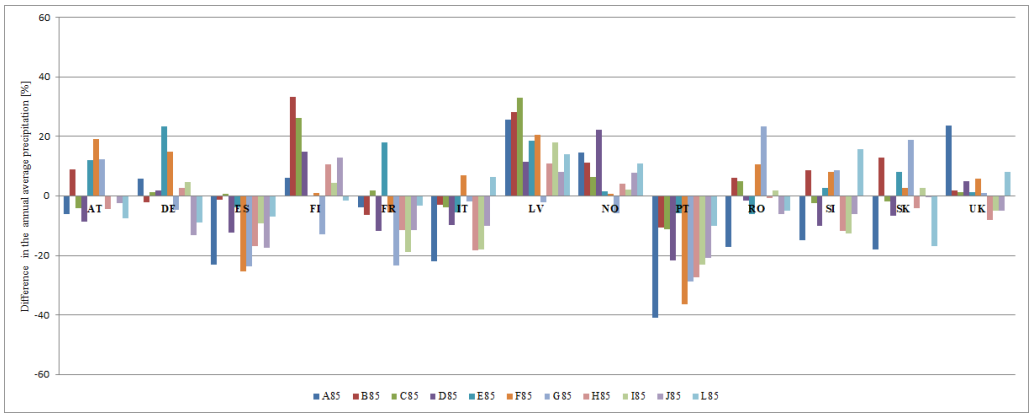

(a) 2030

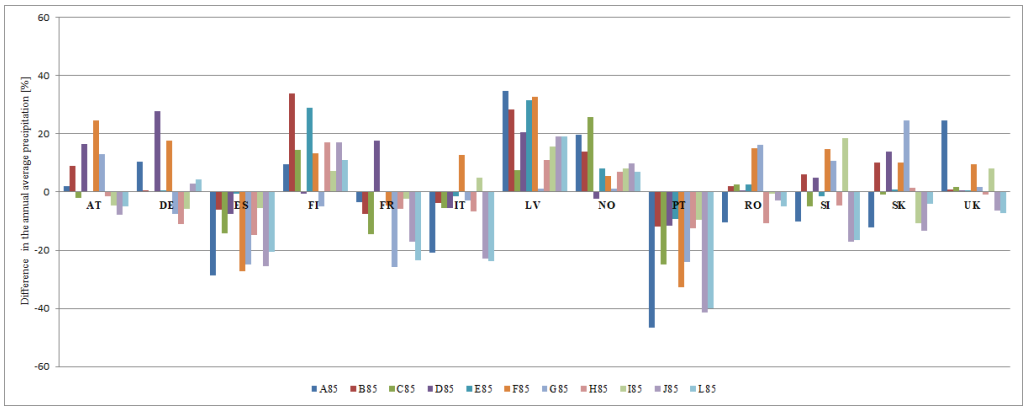

(b) 2050

Figure 3: Difference in the annual average precipitation per country: comparison 2016 and projections for 2030 and 2050 under RCP 8.5.

In Figures 2 and 3, we show the difference in the annual average temperature when our projections under RCP 8.5 are compared with the values in 2016. The comparison here is taken with respect to 2016 and not with a longer historical period, in order to be coherent with the hydropower generation analysis, which is carried on considering the same reference year. This choice is linked to the lack of historical energy data. In these figures, we only consider the countries with installed capacity bigger than 2 GW. Difference for RCP 4.5 can be found in A. It is important to mention that our climate projections represent different possible future trends regarding climate evolution. For instance, we may have a drier PT with almost less 50% of annual precipitation in scenario A85 or even an increase up to 25% in scenario G45 when compared with 2016. Indeed, despite the updated and detailed information on climate projections estimated from GCMs/RCMs, considerable uncertainties are involved, either resulting from the unknown future evolution of GHG concentrations and other forcing agents of the climate system, as well as climate model simplifications of the chaotic behavior of the climate system [24, 25, 26].

3 Methodology

3.1 Machine learning algorithms

Machine learning has been gaining more and more importance in many areas of science, finance and industry [27]. Typically it is used to predict an outcome based on a set of features. In the case of the present paper, the outcome is the capacity factor of the run-of-river hydropower generation and the features are the climate variables. The workflow of ML procedure is given in Figure 4.

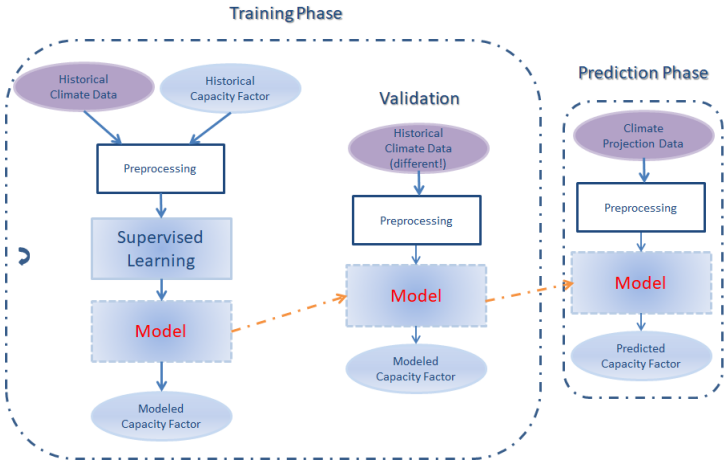

Figure 4: Machine learning workflow.

The procedure starts by training a so-called (supervised) learner with a set of data including the observed outcome and feature measurements. This leads to build a model, which enables predicting the unobserved outcome based on a different set of input features. A good learner is one that accurately predicts such an outcome. In the statistical literature, the features are often called the predictors or the inputs, whereas the outcomes are called the responses or the outputs. Along this paper, we will make use of all these terms. Based on an evaluative metric such as the correlation coefficient, the adjusted coefficient of determination, the mean absolute and mean square percentage errors, to be defined in Section 3.3, we will apply and compare five ML algorithms with the aim at determining a model of highest accuracy.

We use five regression methods: Linear Regressor (LR) [27], Support Vector Machine (SVM) [28], Boosted Ensemble of Trees (BT) [29] and Random Forests (RF) [30]. The four regression methods are implemented in the Statistics and Machine Learning Toolbox 11.4 [31]. In the following, we give a few details of the algorithms cited above.

The most simple algorithm is the linear regression, which consists of finding the best-fitting line through the points of input and response variables. The best-fitting line is called a regression line. The most common type of linear regression is obtained by minimizing a loss function which is the squared error between the observed values and the linear combination of the inputs.

In SMV regression, the goal is to find a function that has at most ϵ deviation

from the target points for all the training data and at the same time is as flat as possible. SVM regression uses a type of loss function called 'insensitive' which was proposed by Vapnik [32]. This function defines a ϵ-tube so that if the predicted value is within the tube the loss is zero, while if the predicted point is outside the tube, the loss function is the magnitude of the difference between the predicted value and the radius ϵ of the tube. The optimization problem derived in [32] is solved by considering its dual formulation. Nonlinearities are then added to the SVM algorithm by mapping the training patterns onto a high-dimensional feature space using some fixed nonlinear functions (kernels). It is well known that SVM regression performance (estimation accuracy) depends on a good setting of hyper parameters, which are the regularization constant used in the definition of the objective function, the width ϵ of the insensitive zone and the kernel parameters.

The RF algorithm is based on an ensemble of decision trees. Random vectors are used for growing each tree in the ensemble. A tree is grown by considering a random selection of training set. Then each tree depends on the values of a random vector sampled independently and with the same distribution for all trees in the forest. In [30], it has been proved that a significant accuracy improvement is gained when randomness is introduced for the parameter selection in ensemble of trees.

The BT algorithm is also based on ensemble of decision trees. The difference is that the predictors are not trained independently but in an iterative manner: every training instance gets a weight assigned that is adapted in every iteration when a new predictor is added to the ensemble. Afterwards the prediction quality of the ensemble is tested on the training set instances.

The tuning of the hyper-parameters for all the algorithms is implemented by using the optimization procedure offered by the Matlab toolboxes along with the trial and error approach.

Recently, it has been shown that the ensemble of machine learning techniques may improve the prediction accuracy [5, 33]. The idea goes as follows: one first uses several ML algorithms to obtain the predicted response, then some combination of the algorithms' outputs is built. In this paper, we simply apply a weighted linear combination of the two best methods for each country. Similarly to [33], we consider the weights derived from each model's mean arctangent percentage error (MAAPE), to be defined in Section 3.3, over the validation set and we consider the output of the hybrid method to be

$$\hat{y}_{hyb} = w_1 \hat{y}_{M1} + w_2 \hat{y}_{M2},$$

where $w_i = \frac{MAAPE_i^{-1}}{MAAPE_1^{-1} + MAAPE_2^{-1}}$, $i = 1, 2$ and $\hat{y}_{M1}$ and $\hat{y}_{M2}$ being the outputs of the two ML algorithms with the best accuracy. This means that $\hat{y}_{hyb}$ is obtained by giving more importance, that is a bigger weight, to the algorithm's output with a smaller error.

3.2 Choice of the predictors

The experiments aim at formalizing an ML model of highest accuracy for the prediction of the capacity factor of the run-of-river based hydropower generation at daily level for each EU country.

The first step in the ML workflow is the training phase. Let us indicate with $T_{\text{train}} = \{t_1, ..., t_j, ..., t_N\}$ a given daily spaced time interval, where t_1 and t_N are respectively the initial and final date in the ISO8601 format 'YYYY-MM-DD' and t_j is the j-th day of this interval. We assume that over the training period we collect the data corresponding to

- Month, Day in T_{train}
- Air temperature, i.e., the time series $AT = [AT_{t_1}, ..., AT_{t_N}]$
- Precipitation, i.e., the time series $TP = [TP_{t_1}, ..., TP_{t_N}]$
- Capacity factor of hydropower generation, i.e., the time series $y = [y_{t_1}, ..., y_{t_N}]$.

As we explained above, the effects of the climate data on hydroelectricity generation occur with a certain delay. In order to count that, we enrich the list of inputs by considering that the hydropower generation at a day t_i is influenced by

- the air temperature at the preceding k_1-th day with respect to t_i, where k_1 is computed by considering the lag that maximizes the sample Pearson correlation [34] between the time series of the hydropower generation y and of the air temperature AT, say $\rho(y, AT)$;
- the precipitation at the preceding k_2-th day with respect to t_i, where k_2 is computed similarly to k_1 by considering $\rho(y, TP)$;
- the sum of precipitation in the last $k_2 + 1$ days with respect to t_i, with k_2 defined above;
- the sum of precipitation in the last k_3 days with respect to t_i, where k_3 is the lag which maximizes $\rho(y, sumP)$, with $sumP$ being the moving sum of the precipitation;

Depending on the country, not all the above listed datasets are relevant for the prediction of the hydropower capacity factor. Then, in order to choose if a certain time series is used as input in the ML algorithms, we compute the correlation ρ between this time series and that of the response over the training period. Then, this dataset is added to the list of predictors if $|\rho|$ is bigger than a certain threshold $\bar{\rho}$. This choice was implemented as we observed that adding inputs whose correlation with the response is lower that a chosen threshold does not improve the prediction in terms of the evaluation criteria to be presented below. Moreover, it is well-known that predictors generated as linear combinations of input variables may improve the accuracy of the learner. Then, in this paper, we also add to the input the climate data aggregated considering the national average. A similar list of predictors was used also in [10]; here we consider that the predictors are aggregated not only at country level but also at regional one.

Once the predictors are selected, these are used for training a learner. The way of learning depends on the ML algorithm selected. We use the ML algorithms presented in Section 3.1, and we generate several models for determining the one which provides the highest accuracy.

3.3 Model evaluation

In this section, we introduce the criteria selected for evaluating the prediction accuracy of the ML algorithms.

We are now in the second part of the ML workflow in Figure 4. Once a model has been built, we can use it for the prediction of the response by considering a new dataset of features. These features are of the same type of the inputs described above, but corresponding to the time interval chosen for the prediction. For instance, if the time series of the air temperature over the training period was used for the generation of the model, now the time series of the air temperature over the new time interval will be used for the prediction. We set the lags k_i, $i = 1, .., 4$ to the values computed in the training phase. The main difference here is that the input list does not include the time series of the hydropower generation, which instead will be the final output of this second phase.

As in this section we wish to measure the prediction accuracy of the ML algorithms, we will perform the second phase of the ML workflow over a time interval in which the time series of the response is actually known. We call $T_{\text{test}} = \{\tau_1, ..., \tau_M\}$ this daily spaced time interval and we indicate with $\bar{y} = [\bar{y}_{\tau_1}, ..., \bar{y}_{\tau_M}]$ the time series of the observed capacity factor over this testing period. From now on, we will use the term 'modeled' instead of 'predicted' output for the results of the ML process, which we indicate as $\hat{y} = [\hat{y}_{\tau_1}, ..., \hat{y}_{\tau_M}]$. It is important to highlight that the testing period is distinct from T_{train} and that $\bar{y}$ is not used as input to the model, but it will be used only for reason of comparison.

For the performance evaluation of the regression models used in this report, we consider the following measures:

- **Correlation coefficient (R)**

$$R = \frac{cov(\bar{y}, \hat{y})}{\sigma_{\bar{y}} \sigma_{\hat{y}}},$$

  where cov is the covariance, and $\sigma_{\bar{y}}$ and $\sigma_{\hat{y}}$ are the standard deviation of $\bar{y}$ and $\hat{y}$, respectively. It is a measure of the strength and direction of the linear relationship between the observed and the modeled variables.

- **Adjusted R-squared** ($\bar{R}^2$)

$$\bar{R}^2 = 1 - (1 - R^2) \frac{M - 1}{M - m - 1},$$

  where M is the number of observations, m is the number of predictors and R^2 is the determination coefficient, that is the square of the correlation coefficient. It compares the explanatory power of regression models that contain different numbers of predictors. The adjusted R-squared is a modified version of R^2 that has been adjusted for the number of predictors in the model.

- **Mean Arctangent Absolute Percentage Error** (MAAPE)

$$MAAPE = \frac{100}{M} \sum_{i=1}^{M} \arctan \left(\left| \frac{\hat{y}_i - \bar{y}_i}{\bar{y}_i} \right| \right)$$

- **Symmetric Mean Absolute Percentage Error** (sMAPE)

$$sMAPE = \frac{100}{M} \sum_{i=1}^{M} \left| \frac{\hat{y}_i - \bar{y}_i}{0.5(\bar{y}_i + \hat{y})} \right|$$

  Note that we preferred to use MAAPE [35] and sMAPE [36] instead of the classical MAPE as the actual capacity factor may include also zero or close to zero values, then MAPE yields extremely large percentage errors.

4 Results

In this section, we compare the performance of the machine learning algorithms mentioned above. This will guide us in the choice of the most suitable model to be used for the long-term prediction of the RoR hydropower capacity factor.

4.1 Modeling the one-year-ahead hydropower capacity factor

We set the training period T_{train} with $t_1 = 2015\text{-}01\text{-}01$ and $t_N = 2018\text{-}12\text{-}31$, whereas for the testing period T_{test} we set $\tau_1 = 2019\text{-}01\text{-}01$ and $\tau_M = 2019\text{-}10\text{-}31$. For each ML algorithm, we generate a model which is used for computing the capacity factor over the period T_{test}.

In Figures 5, 6, 7, 8, 9, and 10(a)-(c), we report the comparison of the observed and the modeled time series of the hydropower capacity factor both in the training and the testing phases for some European countries with installed capacity bigger that 2 GW. The modeled capacity factor is the one corresponding to the ML model with the best performance, see Table 11.

Figures 5, 6, 7, 8, 9, and 10(b)-(d) show the scatter plot of the output models and the observed capacity factor. We indicate with blue dots the values in the period December-January-February (DJF), with orange circles the values in the period March-April-May (MAM), with red dots for June-July-August (JJA) and, finally, with green circles for September-October-November (SON).

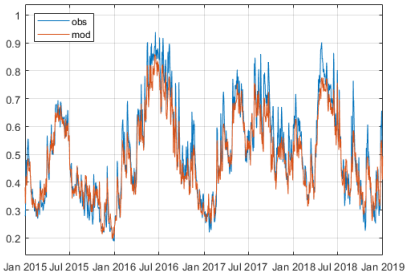

(a)

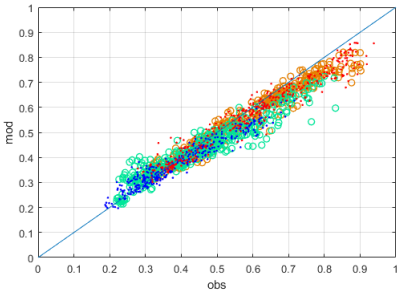

(b)

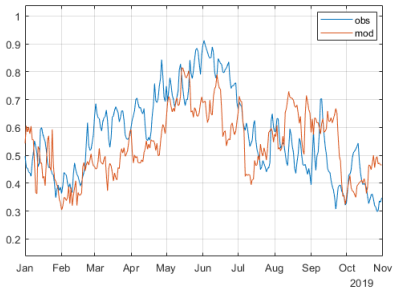

(c)

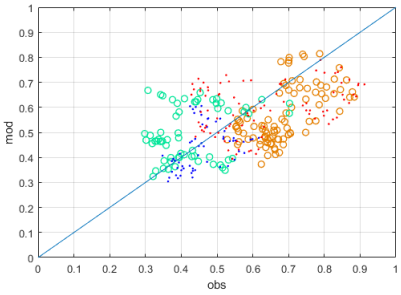

(d)

Figure 5: Country: AT. (a)-(c): Time series of the observed and modeled capacity factor in the training and testing phases, respectively. (b)-(d): Scatter plot of the modeled and observed capacity factor in the training and testing phases, respectively.

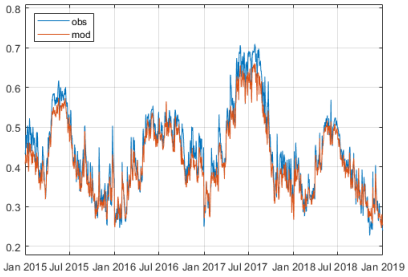

(a)

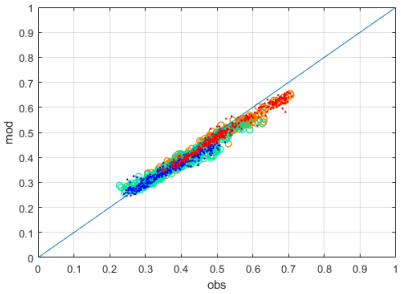

(b)

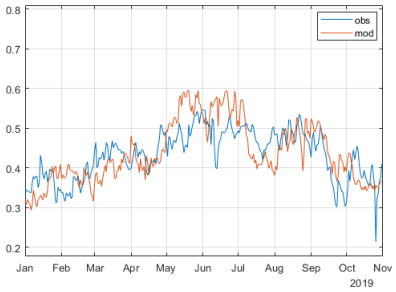

(c)

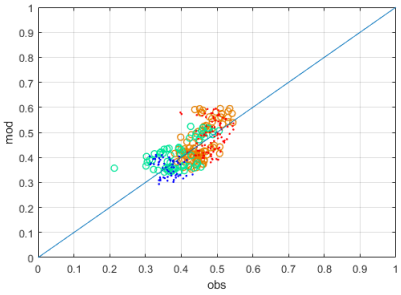

(d)

Figure 6: Country: DE. (a)-(c): Time series of the observed and modeled capacity factor in the training and testing phases, respectively. (b)-(d): Scatter plot of the modeled and observed capacity factor in the training and testing phases, respectively.

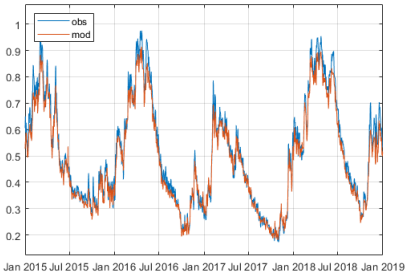

(a)

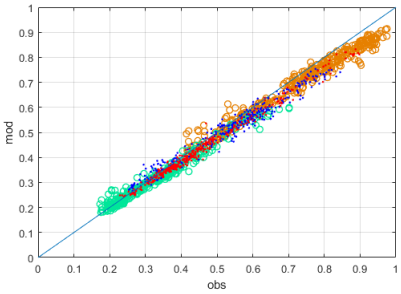

(b)

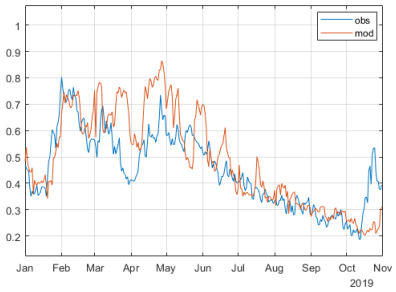

(c)

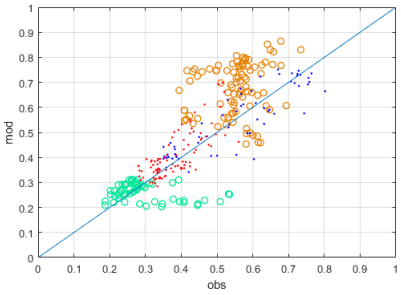

(d)

Figure 7: Country: ES. (a)-(c): time series of the observed and modeled capacity factor in the training and testing phases, respectively. (b)-(d): scatter plot of the modeled and observed capacity factor in the training and testing phases, respectively.

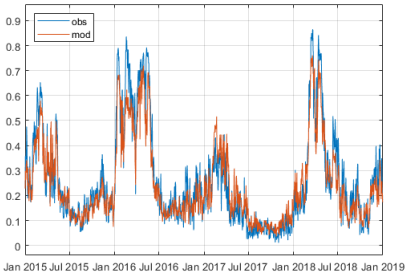

(a)

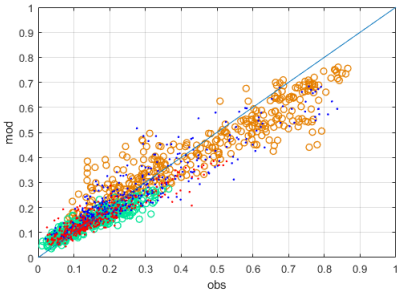

(b)

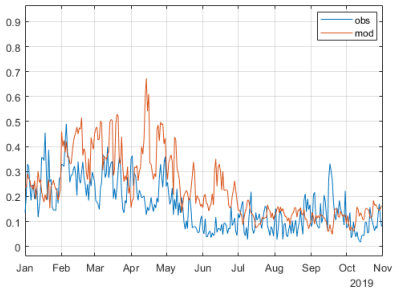

(c)

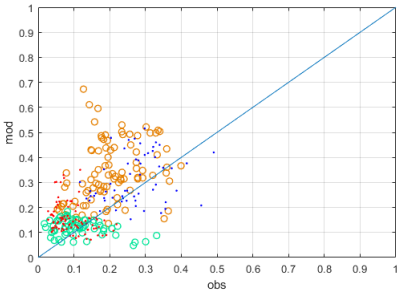

(d)

Figure 8: Country: PT. (a)-(c): Time series of the observed and modeled capacity factor in the training and testing phases, respectively. (b)-(d): Scatter plot of the modeled and observed capacity factor in the training and testing phases, respectively.

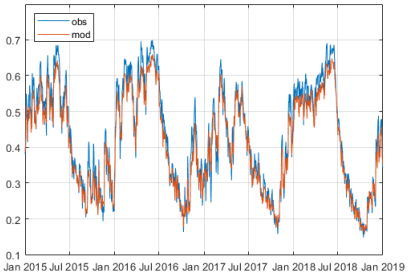

(a)

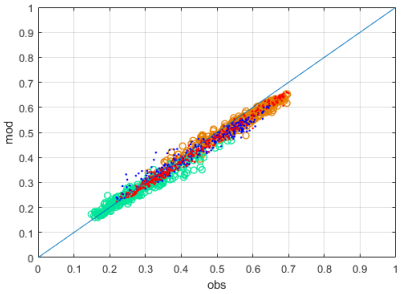

(b)

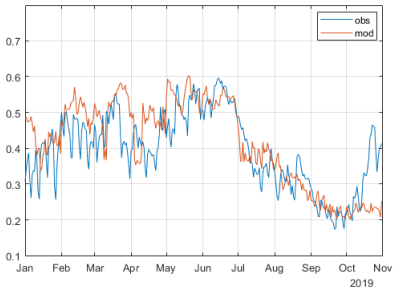

(c)

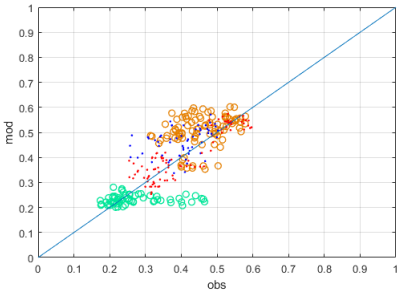

(d)

Figure 9: Country: FR. (a)-(c): Time series of the observed and modeled capacity factor in the training and testing phases, respectively. (b)-(d): Scatter plot of the modeled and observed capacity factor in the training and testing phases.

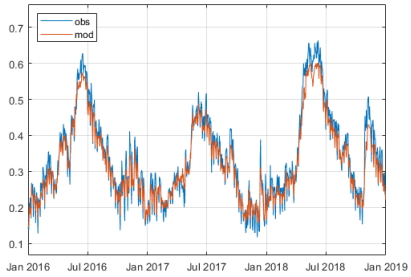

(a)

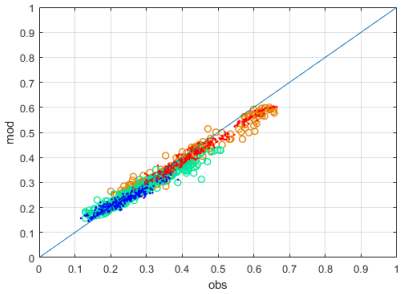

(b)

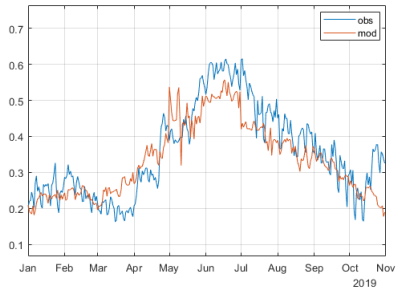

(c)

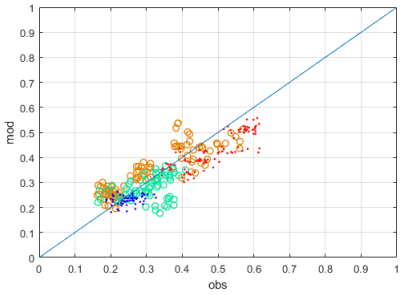

(d)

Figure 10: Country: IT. (a)-(c): Time series of the observed and modeled capacity factor in the training and testing phases, respectively. (b)-(d): Scatter plot of the modeled and observed capacity factor in the training and testing phases. Note that no data are available for the whole 2015, then the training phase is performed only over three years.

We can observe that the modeled response is, in general, quite close to the observed data. In the training phase, the ML models tend to underestimate the capacity factor values when these are greater than 0.6 for all the countries analyzed. This behaviour was also observed in [10]. As shown in Table 11, for countries with relevant RoR installed capacity (> 10 GW), such as Italy and France, we obtain a correlation coefficient equal to 0.87 and 0.7 and $MAAPE = 15.18\%$ and 17.19%, respectively. The worst results in terms of correlation coefficient are for Ireland for which only $R = 0.56$ and $MAAPE = 38.57\%$. It has to be noted that almost 20% of the values for 2017 and 2018 are missing in the ENTSO-E data for this country. We obtain also a lower performance for Portugal ($R = 0.60$ and $MAAPE = 56.04\%$). In fact, in Figure 8, we can notice that also in the training phase, the model is not able to reproduce well the observations. A possible explanation for that is the fact that most of the run-of-river hydropower plants in Portugal are located downstream of large water dams. Then operational decisions affect the flow of the rivers and, consequently, the power generation of RoR plants [37].

The correlation coefficient for the neighboring countries Austria and Germany is about 0.7 with $MAAPE = 16\%$ and $MAAPE = 10\%$, respectively. In the case of Austria, the high values of capacity factors are underestimated by the model also in the testing phase.

A lower accuracy is achieved in the MAM period both in Spain and Portugal. In the latter case, in particular, in Figure 8(d), we can observe that the capacity factor in the MAM period (orange circles) was particularly low if compared with the historical data in 8(c). In order to investigate further this discrepancy with the results obtained with our model, we considered the monthly anomalies of temperature and precipitation in 2019. These are computed as difference between the monthly average temperature (or precipitation) in the testing period and the monthly calendar mean computed over the training period (four years) and given in percentage. By looking at Figure 11, we can see that both in Spain and Portugal, the precipitation values are far from the historical values in the MAM period. In particular, February and March were warmer and drier in 2019. This may cause a lower observed capacity factor in April, which increases only in May with an increment of rain fall. Our models were not able to accurately predict that, probably due to the lack of historical data.

Another issue can be found in the prediction of the capacity factor for the last two weeks of October 2019. Both in Spain and Italy, this month was warmer with respect to the historical period (2015-2018), in particular, the monthly temperature anomaly was almost $+1C$ in Spain and about $+2C$ in Italy, see Figures 11 and 12. The monthly average precipitation was close to the historical period, but exceptional rain falls happened at specific days of this month (21rst-23rd for Spain and 24th for Italy) yielding a fast increase of HP generation in the second part of this month. Finally, also for the case of France, the ML model presents the largest error in the same period. As we can see in Figure 12, October in France registered an exceptional amount of precipitation if compared with average of the four previous years.

As preliminary conclusions of this testing phase, we find the results quite satisfactory considered the limited quantity of available data. The modeled capacity factor is close to the observed values and the performance evaluation in Table 11 is quite good for almost all countries. Yet some particular event could not be well predicted, but we are confident that the accuracy of ML models will

improve with the increase of an historical database to be used in the training phase.

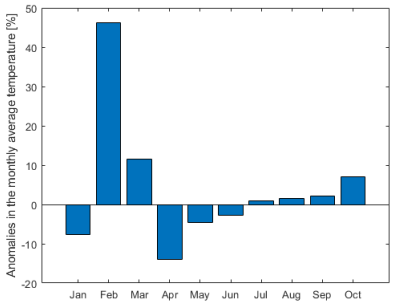

(a) Temperature monthly anomalies - ES

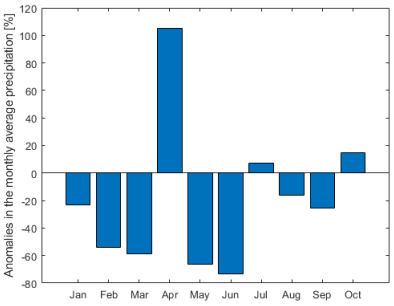

(b) Precipitation monthly anomalies - ES

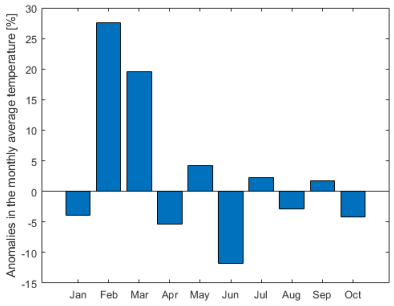

(c) Temperature monthly anomalies -PT

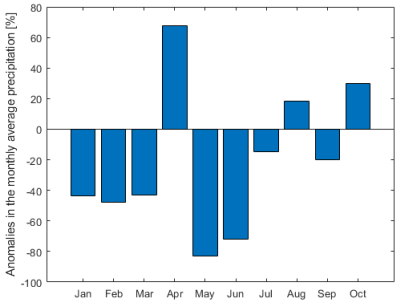

(d) Precipitation monthly anomalies - PT

Figure 11: Countries: ES and PT. Monthly anomalies in the temperature and precipitation over 2019.

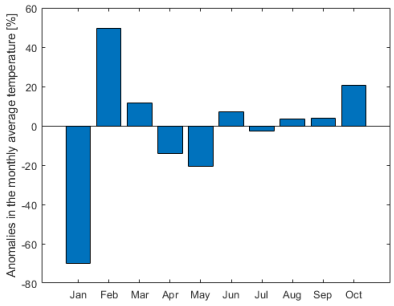

(a) Temperature monthly anomalies - IT

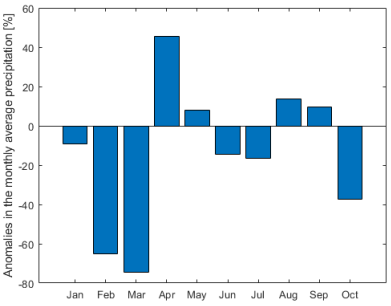

(b) Precipitation monthly anomalies - IT

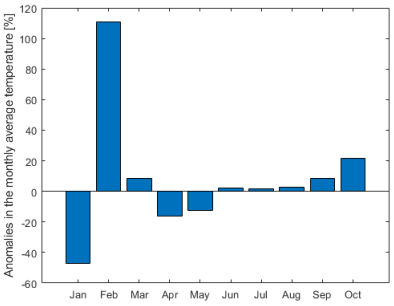

(c) Temperature monthly anomalies - FR

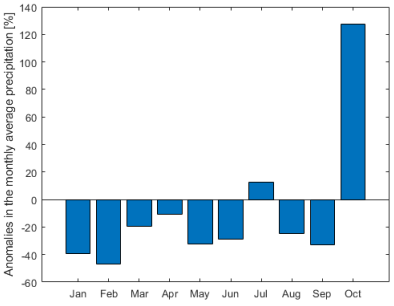

(d) Precipitation monthly anomalies - FR

Figure 12: Countries: IT and FR. Monthly anomalies in the temperature and precipitation over 2019.

4.2 Variability in the long-term prediction of the run-of-river capacity factor

In this section, we present the results obtained by the ML algorithms with the best performance for the long-term prediction of the RoR HP capacity factor. It is worthy to mention also here that the time series of the climate projections used in this paper cannot be considered as an estimation of the year-to-year or season-to-season climate variables. Instead, they are estimations of average conditions. Hence, for the prediction of HP generation over the years 2030 and 2050, for each climate model, we generate time series of hydroelectricity generation as the average over 20 years centered in 2030 and 2050, respectively.

Let us start by considering the difference between the actual annual average RoR HP generation in 2016 and the predicted values for 2030 and 2050. We assume here that the installed capacity remains unchanged and equal to that in 2016. In Figure 13, we show the results obtained for RCP 8.5. Values for other EU countries in both RCP 4.5 and 8.5 are given in the corresponding tables in C. In general, the annual average predicted values are close to the reference year values. In the case of Italy, the increment in HP generation is around $+1\%$. The largest variation in percentage of HP production is forecast for Portugal with a decrease up to -23% for 2030 and -25% for 2050. This is in line with the climate projections of a warmer and dried region for RCP 8.5. Also Spain is expected to have a decrease up to -3% in 2030 and -5% in 2050. The results obtained for Austria and France show a big variability among the possible scenarios. The interval of variation goes from -2% to -12% in 2030 and -3% to -14% in 2050.

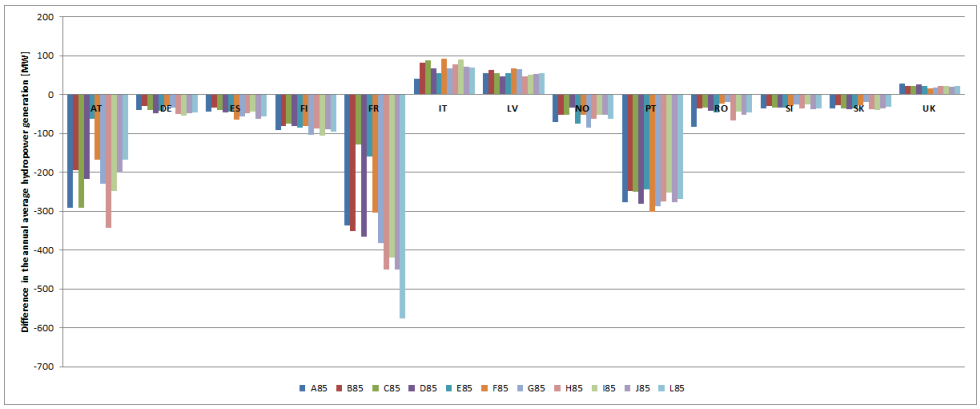

(a) 2030

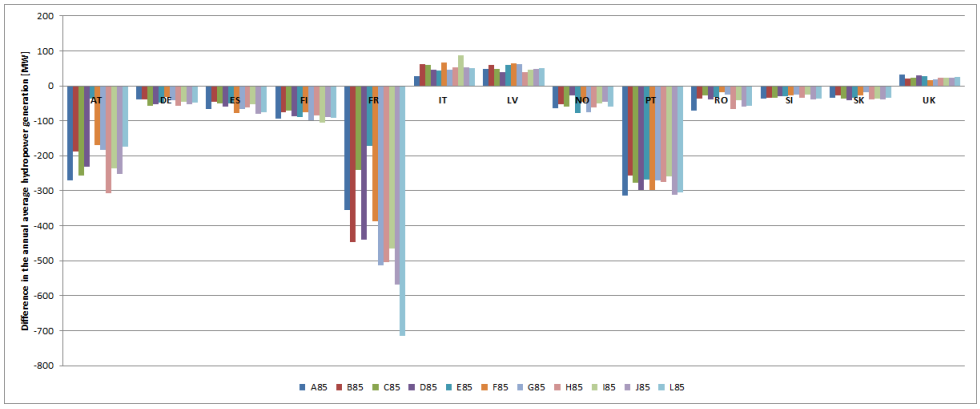

(b) 2050

Figure 13: Difference in the annual average hydropower generation per country: comparison 2016 and predictions for 2030 and 2050 under RCP 8.5.

Yet there are strong limitations of using only these average behaviors for future power generation assessment in Europe. In fact, to give a coherent picture of the future variability in HP generation in each country we need to consider the calendar variability of capacity factors, the variability induced by the different future climate models, and the variability associated to the sliding window of 20 years around each target year.

As an example, we show the time series of the capacity factor and of the precipitation along 20 years centered in 2030 and 2050 for some of the EU countries with large installed hydropower capacity as Austria, France, Portugal and Italy. The results shown in Figures 14, 15, 16 and 17 are obtained by considering the climate projection model $A85$. From this figures, we can see that the largest variability is found in MMA period in Portugal and SON period in France. In particular, in the first case, the capacity factor values are within the interval 0.3-0.7. This is in line with the range of variation found also in the observations for the same period as shown in Figure 8(b). The lowest values are achieved during JJA period, when we also observe a small variability of the precipitation for all the 20 years. Note also that the predicted 20-year average

capacity factor is 10% smaller than the one in the reference year 2016. For the case of France, SON is the most uncertain period for precipitation as shown in Figures 15(e)-(f). This yields a larger interval of variation for the capacity factor between 0 to 0.4. The amplitude of the variation interval for Austria and Italy remains almost uniform along the target years. As depicted in Figures 5 and 10, these amplitudes are about 0.2 for Austria and 0.08 for Italy.

It is interesting to show how the variability of the hydropower generation reflects that of the climate projections. In order to have a deeper insight of that, let us consider the country that showed to have the largest interval of variations, e.g., Portugal. We select now the climate projection model 'F' and we are interested in showing how the HP capacity evolves from 2030 under RCP 4.5 to 2050 under RCP 8.5 based on the precipitation projections. At this aim, we report in Figure 18, the boxplots built by considering the weekly average of the 20-year window data centered in 2030 (or 2050). The blue dots are the weekly average values in the reference year 2016. The computed values of the capacity factor are presented in Figure 18(a)-(b), while the precipitation values are given in Figure 18(c)-(d). First of all, we can see that both in 2030 F45 and 2050 F85 the maximum values of the predicted capacity factor are smaller than those in 2016 for the period going from May to October. The reason for a bigger decrease of hydropower production in the last scenario could be understood by looking at the values of precipitation. Indeed, the first part of the year 2050 shows a smaller variability in the precipitation with few outliers and 90% of data points distributed below the value of $10\,\mathrm{mm}$. We also observe a smaller variability in the dried season, so as observed for the capacity factor.

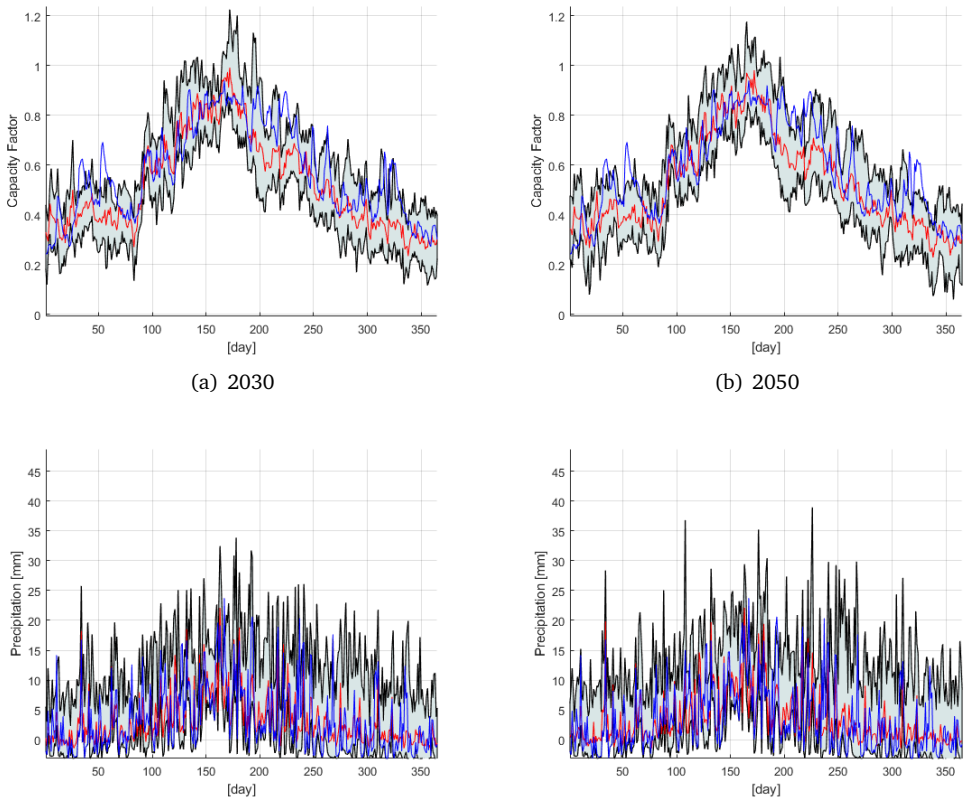

(a) 2030 (b) 2050

(c) 2030 (d) 2050

Figure 14: Country: AT. Variability of the capacity factor and precipitation along 20 years: maximum and minimum envelops (black), calendar mean of the 20-year time series centered in 2030 (or 2050) (red), and observed values in 2016 (blue).

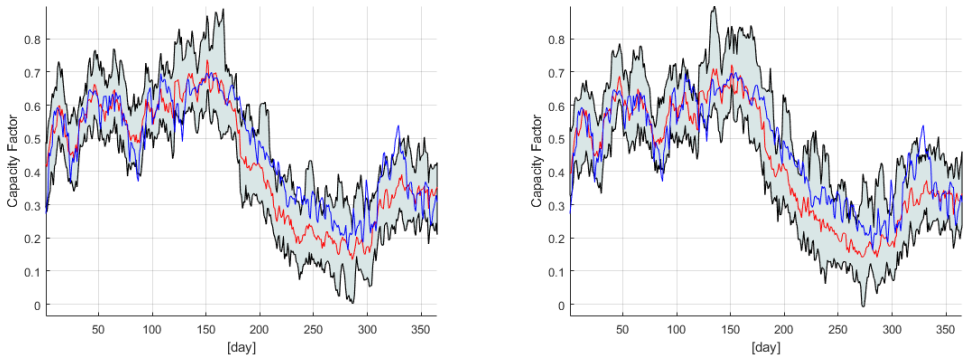

(a) 2030 (b) 2050

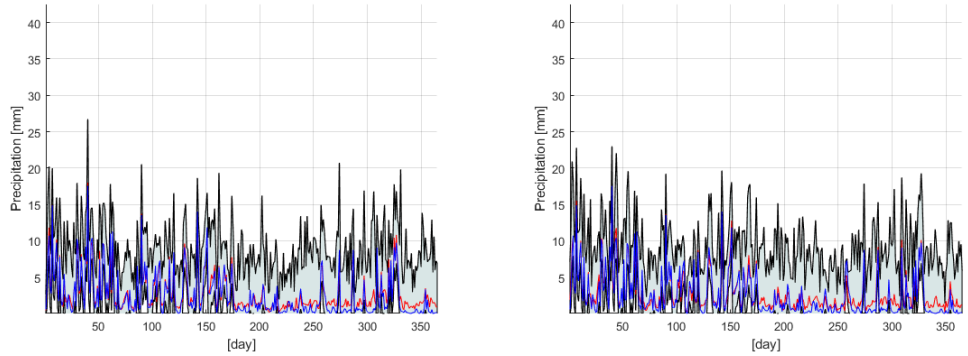

(c) 2030 (d) 2050

Figure 15: Country: FR. Variability of the capacity factor and precipitation along 20 years: maximum and minimum envelops (black), calendar mean of the twenty-year time series centered in 2030 (or 2050) (red), and observed values in 2016 (blue).

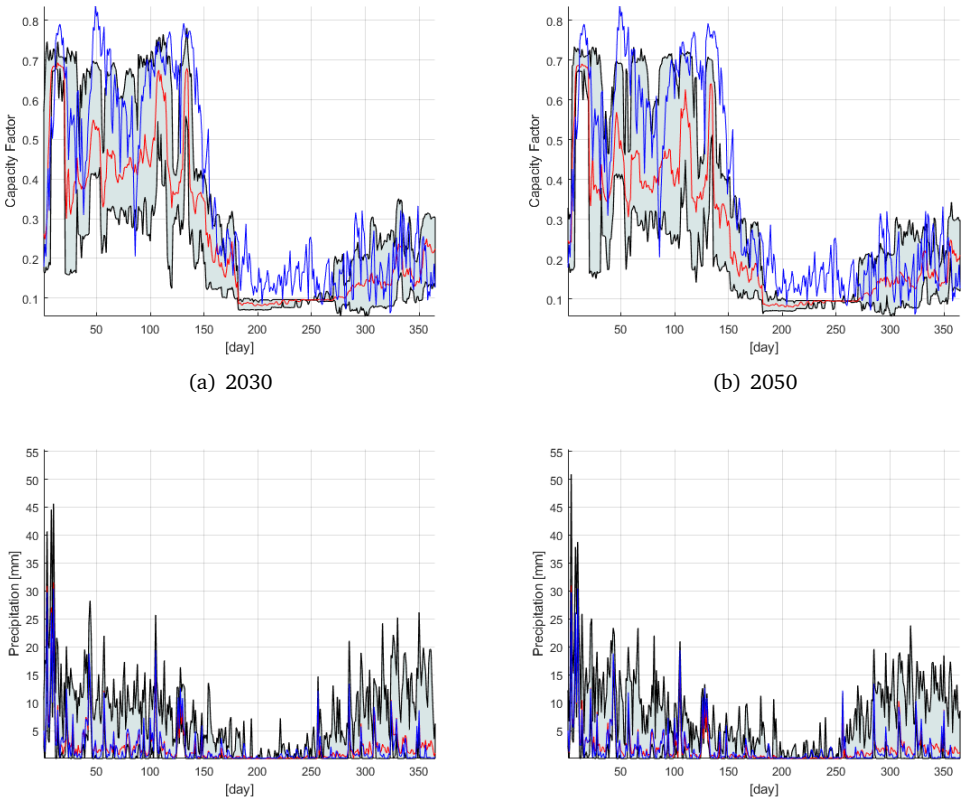

(a) 2030 (b) 2050

(c) 2030 (d) 2050

Figure 16: Country: PT. Variabily of the capacity factor and precipitation along 20 years: maximum and minimum envelops (black), calendar mean of the twenty-year time series centered in 2030 (or 2050) (red), and observed values in 2016 (blue).

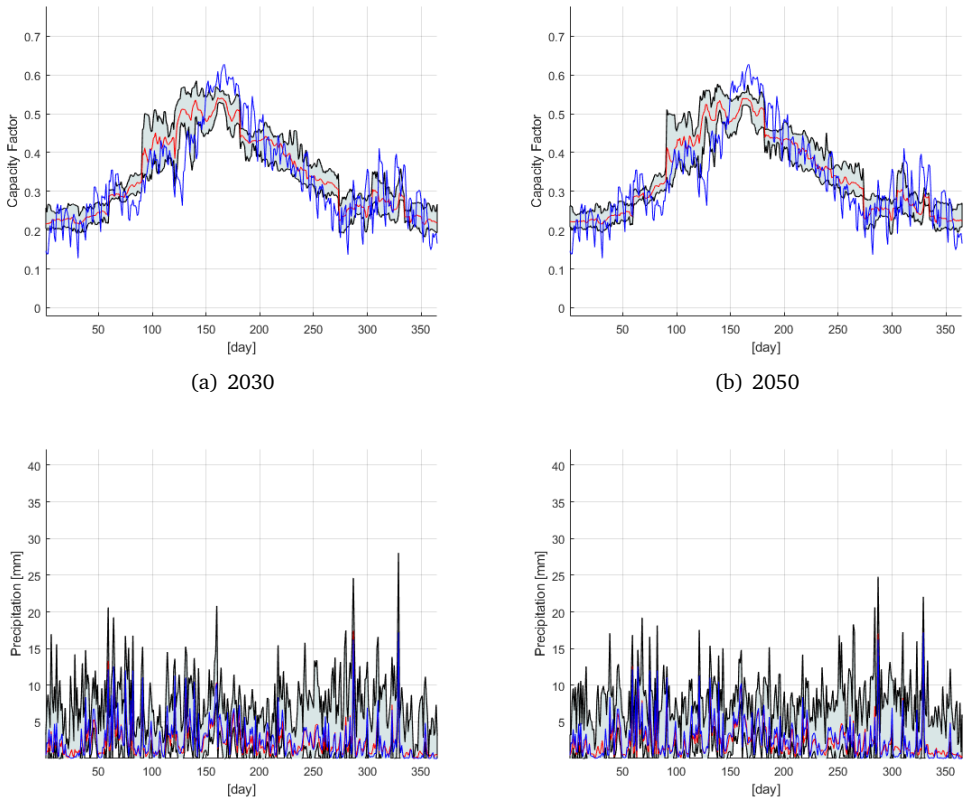

(a) 2030 (b) 2050

(c) 2030 (d) 2050

Figure 17: Country: IT. Variability of the capacity factor and precipitation along 20 years: maximum and minimum envelops (black), calendar mean of the twenty-year time series centered in 2030 (or 2050) (red), and observed values in 2016 (blue).

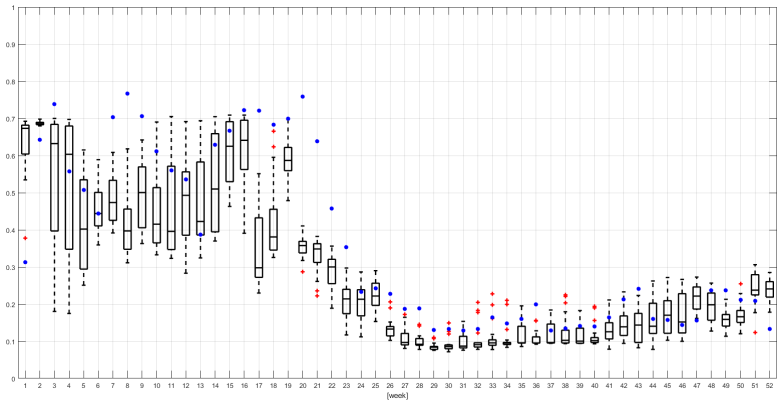

(a) Capacity factor F45 (2030)

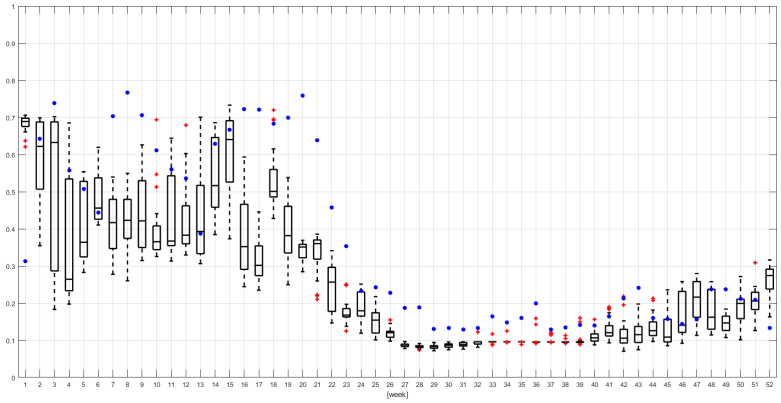

(b) Capacity factor F85 (2050)

4.3 Accessing the worst case scenarios

As we mentioned, the results produced in this paper will be used as input in energy system models for analyzing the climate influence on the optimal operation of power systems. From the point of view of optimal energy planning problem, beside the value of the capacity factor obtained averaging over the twenty-year window centered in 2030 and 2050, it is also interesting to have access to the worst case scenario. In the case of the present paper, this corresponds to the minimum annual average capacity factor computed over the twenty predicted time series. In Figure 19, we depict the worst case capacity factor obtained for each one of the climate models and the values of the observed capacity factor in the reference year. Also from this perspective, we can see that Portugal is expected to be the most impacted by climate changes as the daily time series of the eleven scenarios are all smaller than the observed capacity factor almost for every day of 2050. Yet a high variability among the different scenarios is found in this country in the first five months of the year where the values vary from 0.2 to 0.7. Still staying with the Iberian Peninsula, we can see a decrease of more than 10% of the Spanish capacity factor in the dried period starting in June. For France and Austria, the minimum values of the capacity factors for each models fall below the ones in the reference year in the second part of the year (begin-

ning of July to the end of November). This can be also observed in the winter period in Germany (November-December) and Norway (January-March).

Once again we highlight the diverse possible scenarios involving the different countries. Our methodology offers to power systems' stakeholders and energy system modelers the possibility of addressing the variability of the hydropower production under the future climate conditions described in this paper.

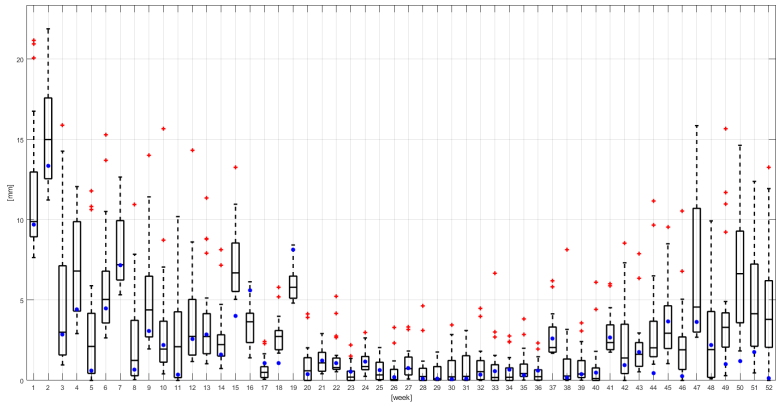

(c) Precipitation F45 (2030)

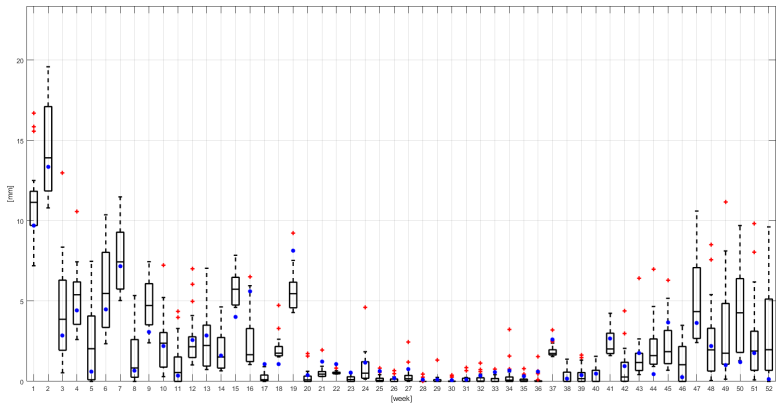

(d) Precipitation F85 (2050)

Figure 18: Country: PT. Variability of the capacity factor and precipitation along 20 years corresponding to the climate models F45 for 2030 and F85 for 2050.

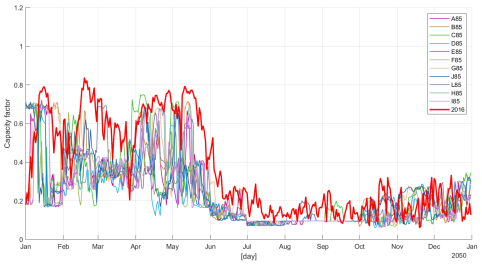

(a) PT

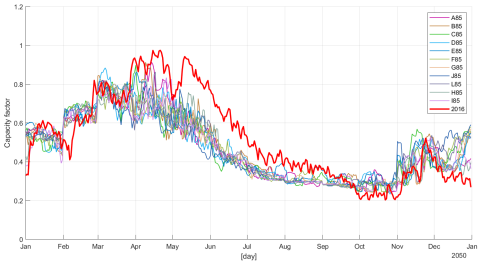

(b) ES

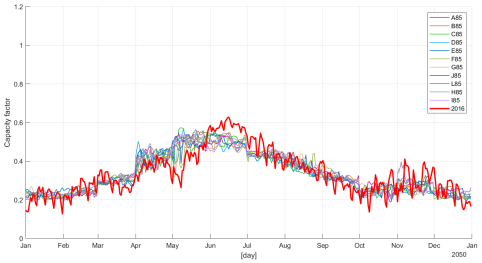

(c) IT

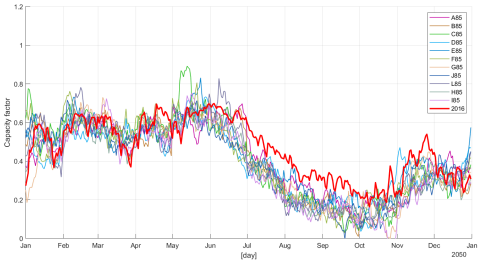

(d) FR

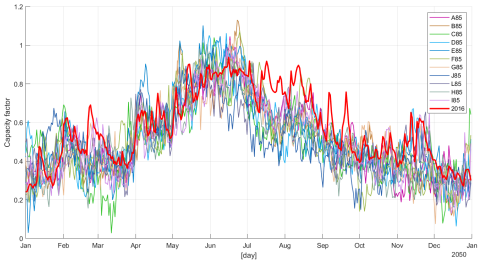

(e) AT

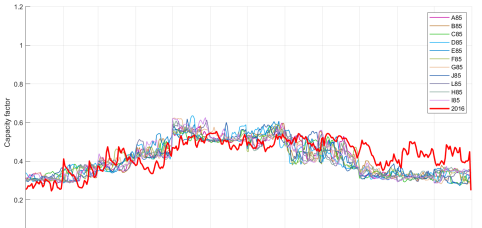

5 Conclusion

Europe is expected to strongly expand its wind and solar power capacity by 2050 to meet its climate goals. In an interconnected system, balancing these highly intermittent sources by hydropower will also involve a European wide evaluation of the variability of hydropower generation for future climatic conditions.

The methodological framework described in this paper offers the possibility of addressing this issue. The two main ingredients are: the formalization of an accurate model and the long-term climate forecasts.

The models are built to translate time series of climate variables into time series of hydropower capacity factor. At this aim, we investigate the performance of several machine learning (ML) methods. The testing phase showed that ML has a good performance in modeling the hydropower capacity factor for almost all European countries. Some errors observed in this phase are due to the lack of historic hydropower generation data. Although this is an important issue now, it will be naturally fixed with time and the methodology used in this paper will still hold and earn more value.

Climate projections are from EURO-CORDEX and consist of 11 models and two RCP scenarios, .i.e., 4.5 and 8.5. The accurate choice in the selection of the models combination allows expressing the variability of the climate behavior for the target years 2030 and 2050.

The combination of ML models and climate projections provide an overview of the long-term variability of capacity factors at country scale for Europe. The results show, in general, a decrease of hydropower in both RCP 4.5 and 8.5. The strongest impact of the temperature increase on the RoR hydropower production, we found in the Western South Europe. In particular, in the Iberian Peninsula, our result show a reduction up to -25% in Portugal and -5% in Spain for 2050 RCP 8.5. A high variability among the several scenarios is shown by the central western countries such as Austria and France with a decrease up to 14% 2050 under RCP 8.5.

Although there are still limitations in this work, it represents a first attempt to access the variability of the future climate scenarios on the run-of-river hydropower production. Our results should be seen as possible realizations of hydropower generation scenarios related to possible future climate conditions.

Future works will be dedicated to the model of the uncertainty of the long-term projections of the daily RoR hydropower generation. The idea is to build a stochastic model for this uncertainty whose dynamics aim to reproduce the statistical characteristics of the prediction deviation with respect to its modeled long-term mean, and so be able to enrich the ML prediction with probabilistic anomalies indicators aggregated at the scale of countries.

Acknoledgements

This research was supported by the Europen Clim2power project. Project CLIM2POWER is part of ERA4CS, an ERA-NET initiated by JPI Climate, and funded by FORMAS (SE), DLR (DE), BMWFW (AT), FCT (PT), EPA (IE), ANR (FR) with co-funding by the European Union (Grant 690462).

A Climate projections

Table 3: Difference in the annual average precipitation: historical values in 2016 [mm] and projections [%] for 2030 under RCP 4.5.

Country	**2016** [mm]	**A45** [%]	**B45** [%]	**C45** [%]	**D45** [%]	**E45** [%]	**F45** [%]	**G45** [%]	**J45** [%]	**L45** [%]	**H45** [%]	**I45** [%]
AT	3.47	-4.32	1.73	-1.44	4.61	13.26	-13.26	6.92	-0.29	5.19	0.00	-10.37
BE	2.67	14.98	-3.75	6.37	-15.73	4.87	-0.75	23.22	25.84	3.75	-3.75	-5.62
BG	2.33	-14.16	5.58	6.44	-3.00	5.58	11.59	16.31	-11.59	1.72	2.58	4.72
CH	4.59	-5.45	-3.92	3.27	-1.09	17.65	3.27	13.73	11.55	0.22	-2.61	-10.68
DE	2.81	6.05	1.42	19.93	-16.01	12.81	-11.03	14.23	23.13	3.56	-2.85	-9.25
ES	1.61	-13.66	-7.45	-1.24	-4.35	1.24	22.98	32.92	-7.45	-18.63	6.83	-3.11
FI	1.80	17.22	11.11	28.33	5.00	11.11	-4.44	-11.67	6.67	2.22	1.11	1.11
FR	2.56	6.64	-7.81	7.81	-10.16	3.91	20.31	37.89	19.92	-2.73	-4.30	3.91
HU	2.22	7.21	5.86	4.50	-1.35	17.12	3.15	13.51	-13.06	4.05	1.35	10.81
IE	2.57	1.56	13.62	19.07	-8.17	-11.28	-17.12	-19.07	0.39	-0.78	-0.78	-8.17
IT	2.68	-15.30	-10.45	-10.07	6.34	8.21	11.94	27.61	-6.72	-4.10	4.48	3.36
LT	2.11	39.34	21.33	3.32	-4.27	9.95	-6.64	-14.22	11.85	-10.90	1.42	-7.58
LV	1.84	29.35	24.46	17.93	-7.07	7.61	-9.78	-23.37	15.22	0.00	8.70	5.98
NO	3.11	0.64	0.32	3.86	-3.54	2.57	-8.68	-9.97	8.04	-6.75	-0.32	-2.25
PL	2.12	29.72	20.28	11.79	5.19	12.74	-7.08	-10.85	2.36	11.79	6.60	-2.83
PT	2.08	3.37	9.13	20.67	2.40	-7.21	-25.00	25.96	-16.83	-9.13	11.54	6.73
RO	2.79	-7.17	4.66	5.02	-8.60	4.66	3.94	26.88	-8.60	11.83	5.73	6.45
SI	2.97	-1.35	1.68	3.37	-8.42	3.03	-2.69	31.99	-5.72	-9.76	-0.67	-1.01
SK	2.24	6.25	9.38	1.79	10.27	8.04	-2.23	4.46	-2.23	2.23	11.16	15.18
UK	2.23	9.87	24.22	17.94	-8.52	-11.21	-15.70	-8.52	10.76	-1.79	-4.48	-2.24

Table 4: Difference in the annual average precipitation: historical values in 2016 [mm] and projections [%] for 2030 under RCP 8.5.

Country	**2016** [mm]	**A85** [%]	**B85** [%]	**C85** [%]	**D85** [%]	**E85** [%]	**F85** [%]	**G85** [%]	**J85** [%]	**L85** [%]	**H85** [%]	**I85** [%]
AT	3.47	-6.05	8.93	-4.03	-8.65	12.10	19.02	12.39	-2.31	-7.49	-4.32	0.00
BE	2.67	9.36	-11.61	-4.12	11.99	14.23	15.73	-6.74	-13.86	-7.87	2.62	-6.37
BG	2.33	-20.17	-4.72	10.30	4.29	-10.30	2.58	8.15	-1.29	3.86	8.15	-6.44
CH	4.59	-3.92	7.63	12.42	-8.28	22.00	8.28	-7.19	-14.38	-6.75	-10.68	-8.71
DE	2.81	5.69	-2.14	1.42	1.78	23.49	14.95	-4.63	-13.17	-8.90	2.85	4.63
ES	1.61	-22.98	-1.24	0.62	-12.42	-3.73	-25.47	-23.60	-17.39	-6.83	-16.77	-9.32
FI	1.80	6.11	33.33	26.11	15.00	0.00	1.11	-12.78	12.78	-1.67	10.56	4.44
FR	2.56	-3.91	-6.25	1.95	-11.72	17.97	-5.47	-23.44	-11.33	-3.13	-11.33	-18.75
HU	2.22	-17.12	14.86	3.15	1.80	8.56	-8.11	15.32	-11.71	-13.06	-6.76	7.66
IE	2.57	18.29	3.50	-1.17	14.79	0.39	4.28	-2.33	-0.39	12.45	-11.28	-0.78
IT	2.68	-22.01	-2.99	-3.73	-9.70	-5.60	7.09	-1.87	-10.07	6.34	-18.28	-17.91
LT	2.11	10.43	32.70	18.48	5.69	30.81	22.27	7.11	4.27	-1.90	6.16	8.53
LV	1.84	25.54	28.26	33.15	11.41	18.48	20.65	-2.17	8.15	14.13	10.87	17.93
NO	3.11	14.47	11.25	6.43	22.19	1.61	0.64	-5.79	7.72	10.93	4.18	2.25
PL	2.12	-10.38	32.08	-2.83	-8.96	16.98	16.04	19.34	-11.79	-12.74	1.42	1.42
PT	2.08	-40.87	-10.58	-11.06	-21.63	-5.77	-36.54	-28.85	-20.67	-10.10	-27.40	-23.08
RO	2.79	-17.20	6.09	5.02	-1.43	-6.09	10.75	23.30	-6.09	-5.02	-0.72	1.79
SI	2.97	-14.81	8.75	-2.36	-10.10	2.69	8.08	8.75	-6.06	15.82	-11.78	-12.46
SK	2.24	-17.86	12.95	-1.79	-6.70	8.04	2.68	18.75	-0.45	-16.96	-4.02	2.68
UK	2.23	23.77	1.79	1.35	4.93	1.35	5.83	0.90	-4.93	8.07	-8.07	-4.93

Table 5: Difference in the annual average precipitation: historical values in 2016 [mm] and projections [%] for 2050 under RCP 4.5.

Country	**2016** [mm]	**A45** [%]	**B45** [%]	**C45** [%]	**D45** [%]	**E45** [%]	**F45** [%]	**G45** [%]	**J45** [%]	**L45** [%]	**H45** [%]	**I45** [%]
AT	3.47	-4.03	3.75	3.46	10.95	-4.90	-10.09	10.09	-1.15	-11.53	-1.15	1.15
BE	2.67	17.98	-6.37	-21.72	-2.25	3.37	1.12	22.10	-7.49	-11.24	25.09	-0.75
BG	2.33	-12.45	6.87	-0.43	9.44	6.87	8.15	10.30	3.00	1.29	-12.45	-3.43
CH	4.59	-2.83	-8.06	-4.79	13.07	-1.74	7.63	15.90	-2.40	-12.20	11.98	-2.18
DE	2.81	7.47	1.78	-18.15	9.61	16.01	-9.61	15.30	-6.05	-12.81	21.71	1.07
ES	1.61	-14.91	-9.94	-6.21	-2.48	-4.97	31.06	34.16	0.00	-10.56	-4.35	-19.88
FI	1.80	20.56	13.33	4.44	11.67	31.11	-5.00	-3.89	5.00	8.89	10.00	10.00
FR	2.56	8.59	-12.89	-14.45	-1.95	1.95	26.17	37.89	-8.20	-0.78	19.53	-3.52
HU	2.22	2.70	8.56	0.90	13.96	0.45	6.76	18.02	-4.95	6.76	-11.26	1.35
IT	2.68	-14.93	-14.18	5.97	7.46	-13.43	15.30	28.73	0.37	0.37	-6.34	-5.60
LT	2.11	36.02	23.70	-5.21	14.69	3.79	-4.27	-10.90	1.42	-8.06	14.69	-8.06
LV	1.84	29.35	27.72	-5.98	9.78	21.20	-6.52	-19.57	13.04	8.70	19.57	4.89
NO	3.11	0.64	2.57	-3.86	1.29	8.04	-6.11	-5.47	3.54	2.25	7.07	-3.86
PL	2.12	30.66	23.11	3.30	14.62	8.02	-5.19	-6.60	0.94	-4.25	5.19	10.85
PT	2.08	2.40	4.81	0.00	-13.46	15.87	38.46	35.10	-3.37	-7.21	-16.83	-9.62
RO	2.79	-5.73	5.73	-6.09	6.09	2.87	2.15	23.66	1.79	3.58	-9.68	9.32
SI	2.97	-2.36	-1.35	-6.40	1.35	-1.68	2.02	37.04	-7.74	-4.71	-3.70	-11.78
SK	2.24	6.70	13.39	8.48	7.59	-2.68	1.79	9.82	2.68	10.27	-1.79	2.23
UK	2.23	10.31	21.08	-13.00	-14.35	15.25	-14.80	-6.73	-8.07	-5.83	9.42	-0.90

Table 6: Difference in the annual average precipitation: historical values in 2016 [mm] and projections [%] for 2050 under RCP 8.5.

Country	**2016**[mm]	**A85** [%]	**B85** [%]	**C85** [%]	**D85** [%]	**E85** [%]	**F85** [%]	**G85** [%]	**J85** [%]	**L85** [%]	**H85** [%]	**I85** [%]
AT	3.47	2.02	8.93	-2.02	16.43	0.00	24.50	12.97	-7.78	-4.90	-1.44	-4.61
BE	2.67	15.36	-10.86	7.12	17.60	-7.49	18.35	-11.24	1.50	-7.12	-10.11	-7.87
BG	2.33	-15.02	-4.29	9.44	-4.29	3.86	-1.29	0.00	7.30	-15.02	-12.02	5.58
CH	4.59	0.65	7.19	-7.19	23.97	15.25	12.42	-11.33	-15.25	-15.47	-11.33	-6.10
DE	2.81	10.32	0.71	0.36	27.76	0.71	17.79	-7.47	2.85	4.27	-11.03	-5.69
ES	1.61	-28.57	-6.21	-14.29	-7.45	-0.62	-27.33	-24.84	-25.47	-20.50	-14.91	-5.59
FI	1.80	9.44	33.89	14.44	-0.56	28.89	13.33	-5.00	17.22	11.11	17.22	7.22
FR	2.56	-3.52	-7.42	-14.45	17.58	0.39	-4.69	-25.78	-17.19	-23.44	-5.86	-2.34
HU	2.22	-9.91	13.06	7.66	13.51	3.60	0.90	17.12	-11.71	1.80	-8.11	-5.41
IT	2.68	-20.90	-3.73	-5.60	-5.60	-1.49	12.69	-2.99	-22.76	-23.88	-6.72	4.85
LT	2.11	18.48	27.01	4.74	33.65	21.33	32.23	7.58	10.43	6.64	7.11	-2.37
LV	1.84	34.78	28.26	7.61	20.65	31.52	32.61	1.09	19.02	19.02	10.87	15.76
NO	3.11	19.61	13.83	25.72	-2.25	8.04	5.47	1.29	9.97	7.07	7.07	8.04
PL	2.12	-5.19	30.66	-6.13	26.89	1.42	23.58	20.28	-1.42	-2.83	-7.55	-6.13
PT	2.08	-46.63	-12.02	-25.00	-11.54	-9.13	-32.69	-24.04	-41.35	-39.90	-12.50	-9.62
RO	2.79	-10.39	2.15	2.51	0.72	2.51	15.05	16.13	-2.87	-5.02	-10.75	-0.72
SI	2.97	-10.10	6.06	-5.05	5.05	-1.35	14.81	10.77	-17.17	-16.50	-4.71	18.52
SK	2.24	-12.05	10.27	-0.89	13.84	0.89	10.27	24.55	-13.39	-4.02	1.34	-10.71
UK	2.23	24.66	0.90	1.79	0.45	0.45	9.42	1.79	-6.28	-7.17	-0.90	8.07

Table 7: Difference in the annual average temperature in Celsius Degrees: historical values in 2016 and projections for 2030 under RCP 4.5.

Country	2016[*C*]	**A45** [*C*]	**B45** [*C*]	**C45** [*C*]	**D45** [*C*]	**E45** [*C*]	**F45** [*C*]	**G45** [*C*]	**J45** [*C*]	**L45** [*C*]	**H45** [*C*]	**I45** [*C*]
AT	6.85	0.74	0.17	0.2	0	-0.5	-0.38	-0.17	0.29	-0.1	0.39	0.88
BE	10.08	0.46	0.7	0.25	0.51	-0.26	-0.3	-0.47	-0.17	0.26	0.6	1.24
BG	11.16	0.75	-0.54	-0.07	-0.45	0.24	-0.44	-0.62	0.86	-0.21	1.37	0.71
CH	6.14	0.81	0.54	0.43	0.17	-0.14	-0.18	-0.03	-0.32	0.01	0.31	0.91
DE	9.16	0.62	0.4	0.22	0.55	-0.24	-0.55	-0.5	0.12	0.19	0.49	1.2
ES	14.22	1.26	0.84	0.75	0.48	-0.07	-0.12	-0.09	-0.18	0.48	0.74	0.94
FI	5.14	-0.25	0.54	0.62	0.64	0.74	-0.56	0.09	1.03	-0.4	0.38	1.05
FR	11.01	0.8	0.76	0.27	0.5	-0.22	-0.08	-0.22	-0.37	0.23	0.83	1.2
HU	10.65	0.46	-0.29	-0.25	-0.42	-0.9	-0.74	-0.59	0.83	-0.05	1.13	0.91
IE	9.75	0.31	0.67	0.67	0.51	0	-0.18	-0.12	-0.49	0.36	0.56	0.89
IT	11.86	0.77	0.38	0.32	0.01	-0.37	0.02	0.05	0.07	0.1	0.48	0.63
LT	7.20	0.1	0.04	0.23	0.51	-0.47	-1.47	-0.81	1.37	-0.42	0.22	1.08
LV	6.86	0.05	0.26	0.41	0.53	0.04	-1.11	-0.63	1.3	-0.54	0.14	0.78
NO	3.55	0.05	0.75	0.42	0.62	-0.24	0.05	0.41	0.66	0.41	-0.1	1.02
PL	8.93	0.27	-0.33	-0.34	0.41	-0.94	-1.24	-0.6	1.07	-0.16	0.62	1.24
PT	13.90	1.84	1.35	1.39	1.95	1.61	0.89	0.98	0.91	1.6	1.81	1.76
RO	9.80	0.41	-0.63	-0.08	-0.39	0.04	-0.82	-0.94	0.97	-0.07	1.33	0.63
SI	9.43	0.52	0.08	-0.03	0.09	-0.86	-0.29	-0.41	0.58	0.24	0.64	0.8
SK	8.65	0.34	-0.38	-0.22	-0.18	-0.96	-0.79	-0.4	0.84	0.09	0.85	1.25
UK	9.81	0.32	0.46	0.53	0.57	-0.05	-0.24	-0.16	-0.3	0.32	0.45	0.91

Table 8: Difference in the annual average temperature in Celsius Degrees: historical values in 2016 and projections for 2030 under RCP 8.5.

Country	**2016** $[C]$	**A85** $[C]$	**B85** $[C]$	**C85** $[C]$	**D85** $[C]$	**E85** $[C]$	**F85** $[C]$	**G85** $[C]$	**J85** $[C]$	**L85** $[C]$	**H85** $[C]$	**I85** $[C]$
AT	6.85	1.33	0.09	0.64	1.13	1.36	-0.93	-0.11	-0.12	1.13	0.72	0.69
BE	10.08	1.2	0.09	0.35	0.99	1.04	-0.71	-0.03	0.07	0.76	1.58	0.9
BG	11.16	1.06	0.71	0.98	-0.2	1.72	0.13	0.25	-0.95	1.62	0.53	0.67
CH	6.14	1.13	0.36	0.53	1	1.19	-0.83	0.21	0.29	0.9	1.09	0.84
DE	9.16	1.27	0.05	0.41	1.19	1.14	-0.95	-0.34	0.2	0.91	1.31	0.73
ES	14.22	0.74	0.3	0.33	0.84	0.56	0.56	0.82	0.59	0.88	1.32	1.03
FI	5.14	1.4	0.25	0.75	2.81	-1.04	-1.01	-1.33	2.26	1.37	1.22	0.79
FR	11.01	0.86	0.5	0.69	0.92	0.88	-0.63	0.31	0.25	0.93	1.61	1.19
HR	11.42	1.19	0.25	0.6	0.75	1.24	-0.51	0.06	-0.09	1.22	1.02	0.79
HU	10.65	1.42	0.02	0.38	1	1.28	-0.73	-0.36	-0.38	1.57	0.68	0.65
IE	9.75	0.81	0.19	0.11	0.33	1.05	-0.46	-0.13	0.62	0.27	0.4	0.48
IT	11.86	1.13	0.46	0.61	0.58	0.95	-0.25	0.39	0.05	0.88	1.07	0.88
LT	7.20	1.69	-0.02	0.45	1.92	-0.06	-1.18	-1.17	1.72	1.17	0.84	0.66
LV	6.86	1.3	0.12	0.56	2.25	-0.34	-1.09	-1.31	2.05	1.25	1.01	0.58
NO	3.55	1.26	-0.25	0.04	1.57	0.03	-0.51	-0.43	1.5	0.93	0.65	0.66
PL	8.93	1.82	-0.39	0.55	1.4	0.87	-1.13	-0.8	0.38	1.02	0.63	0.57
PT	13.90	1.3	1.24	1.28	2.1	1.17	1.65	1.92	1.96	1.57	2.25	2.25
RO	9.80	1.07	0.34	1.04	0.42	1.65	-0.38	-0.17	-0.59	1.72	0.34	0.67
SI	9.43	1.16	0.24	0.64	0.94	1.28	-0.78	-0.01	-0.17	0.98	1.1	1.23
SK	8.65	1.42	-0.09	0.42	1.17	1.18	-0.94	-0.53	-0.24	1.31	0.51	0.7
UK	9.81	0.97	0.2	0.33	0.74	0.81	-0.56	-0.22	0.53	0.57	0.96	0.8

Table 9: Difference in the annual average temperature in Celsius Degrees: historical values in 2016 and projections for 2050 under RCP 4.5.

Country	**2016**$[C]$	**A45** $[C]$	**B45** $[C]$	**C45** $[C]$	**D45** $[C]$	**E45** $[C]$	**F45** $[C]$	**G45** $[C]$	**J45** $[C]$	**L45** $[C]$	**H45** $[C]$	**I45** $[C]$
AT	6.85	1.17	0.59	0.59	-0.36	0.65	0.08	0.49	1.08	1.42	0.34	0.54
BE	10.08	0.86	1.06	1.17	-0.24	0.58	-0.05	0.03	1.49	1.88	-0.12	0.83
BG	11.16	1.05	-0.16	0.09	0.42	0.33	0.54	0.41	1.74	1.05	1.18	0.44
CH	6.14	1.17	1.08	0.69	0.12	0.9	0.14	0.64	0.95	1.48	-0.2	0.66
DE	9.16	1.08	0.78	1.2	-0.28	0.6	-0.18	0.07	1.35	1.85	0.13	0.71
ES	14.22	1.66	1.32	0.94	0.33	1.22	0.23	0.34	1.27	1.46	0.2	1.14
FI	5.14	0.38	0.99	1.51	0.81	0.99	0.16	0.73	1.5	2	0.96	0.26
FR	11.01	1.17	1.22	1.02	0	0.73	0.23	0.29	1.52	1.79	-0.21	0.87
HU	10.65	1.03	0.04	0.29	-0.72	0.37	-0.04	0.12	1.86	1.39	0.83	0.5
IE	9.75	0.51	0.76	1.06	0.12	0.76	-0.24	-0.15	1.05	1.32	-0.3	0.79
IT	11.86	1.1	0.9	0.5	-0.14	0.79	0.47	0.61	1	1.14	0.26	0.71
LT	7.20	0.58	0.42	1.24	-0.52	0.73	-0.83	-0.16	1.33	1.77	1.23	0.11
LV	6.86	0.57	0.66	1.25	0.02	0.85	-0.5	-0.02	1.23	1.54	1.17	0.05
NO	3.55	0.66	1.11	1.44	-0.11	0.81	0.42	0.9	0.86	1.8	0.82	0.71
PL	8.93	0.73	-0.01	1.12	-1.04	0.23	-0.62	0.09	1.61	1.9	1	0.27
PT	13.90	1.41	0.98	1.26	0.81	0.99	0.1	0.26	1.31	1.39	0.29	1.14
RO	9.80	0.82	-0.24	0.16	0.18	0.44	0.12	0.03	1.92	1.07	1.15	0.5
SI	9.43	1.05	0.61	0.6	-0.73	0.48	0.26	0.24	1.41	1.31	0.64	0.95
SK	8.65	0.87	-0.05	0.59	-0.79	0.39	-0.15	0.27	1.6	1.8	0.81	0.55
UK	9.81	0.63	0.65	1.26	0.06	0.68	-0.12	0.05	1.15	1.52	-0.19	0.79

Table 10: Difference in the annual average temperature in Celsius Degrees: historical values in 2016 and projections for 2050 under RCP 8.5.

Country	**2016** $[C]$	**A85** $[C]$	**B85**$[C]$	**C85** $[C]$	**D85** $[C]$	**E85** $[C]$	**F85** $[C]$	**G85** $[C]$	**J85** $[C]$	**L85** $[C]$	**H85** $[C]$	**I85** $[C]$
AT	6.85	1.96	0.83	1.42	1.58	1.76	-0.32	1.27	1.57	1.66	1.09	1.29
BE	10.08	1.85	0.85	1.56	1.36	1.42	-0.21	1.04	2.39	1.76	0.96	1.14
BG	11.16	1.58	1.35	0	2.36	2	1.3	1.55	1.18	1.55	0.98	2.06
CH	6.14	1.74	1.24	1.42	1.55	1.78	-0.16	1.63	1.98	1.87	1.3	1.25
DE	9.16	2.02	0.75	1.69	1.43	1.41	-0.39	0.8	2.14	1.63	1.14	1.19
ES	14.22	1.5	1.21	1.38	1.01	1.4	1.3	1.79	2.26	1.94	1.41	1.46
FI	5.14	2.45	1.08	4.15	-0.46	1.79	-0.02	-0.13	2.46	2.25	2.77	2.19
FR	11.01	1.49	1.4	1.45	1.28	1.92	-0.07	1.44	2.39	2.03	1.16	1.38
GR	15.80	1.44	1.16	0.36	1.66	1.53	1.45	1.5	1.17	1.53	1.06	1.71
HU	10.65	2.01	0.65	1.12	1.55	1.32	-0.15	0.88	1.48	1.52	1	1.59
IE	9.75	1.21	0.8	0.98	1.42	0.81	-0.34	0.18	0.95	1	0.92	0.81
IT	11.86	1.68	1.3	0.99	1.28	1.64	0.53	1.52	1.9	1.86	1.13	1.25
LT	7.20	2.68	0.59	2.6	0.26	1.18	-0.39	-0.25	2	1.84	2.45	1.6
LV	6.86	2.29	0.75	3.08	0	1.37	-0.25	-0.34	2.2	1.83	2.72	1.81
NO	3.55	1.97	0.66	2.82	0.64	1.15	0.14	0.58	1.72	1.79	1.87	1.45
PT	13.90	1.28	1.14	1.58	0.81	1.33	1.3	1.77	2.2	2.08	1.53	1.31
RO	9.80	1.6	1	0.56	2.11	1.93	0.52	1.13	1.1	1.54	1.1	2.01
SI	9.43	1.77	1.04	1.2	1.46	1.69	-0.14	1.3	1.89	2.2	1.11	1.17
SK	8.65	2.12	0.48	1.47	1.4	1.37	-0.37	0.76	1.39	1.61	1.05	1.4
UK	9.81	1.53	0.94	1.51	1.23	1.24	-0.26	0.34	1.62	1.45	1.03	1.03

B Performance of the ML algorithms

In Table 11, we show the values of the evaluation measures obtained in the testing phase by the several ML methods. The column titled MAPEm is the classical MAPE obtained excluding zeros values (smaller that 10^{-3}). We highlight in yellow the two ML algorithms with the best performance.

Table 11: Performance evaluation of the ML algorithms for the computation of the one-year-ahead run-of-river based hydropower capacity factor.

Country	ML	R	$\bar{R}^2$	MAAPE	sMAPE	MAPEm
AT	RF	0.5695	0.2501	19.1438	18.7301	19.9850
	BT	0.5344	0.2070	19.7603	19.8731	20.6018
	SVM	0.5215	0.1919	19.5003	19.4096	20.5558
	LR	0.7147	0.4570	16.2695	16.4476	16.7212
	hyb	0.5497	0.2255	19.3084	19.3332	20.1526
BG	RF	0.8411	0.6693	65.5022	49.2937	96.5644
	BT	0.8313	0.6508	60.6650	45.9549	86.3017
	SVM	0.8350	0.6576	63.1719	47.7868	88.6060
	LR	0.8729	0.7308	65.5586	49.4534	92.7665
	hyb	0.8417	0.6703	61.8055	46.7813	87.1631
CH	RF	0.7392	0.4774	29.2819	28.2731	31.7815
	BT	0.7114	0.4310	27.2893	27.4345	29.3472
	SVM	0.6906	0.3974	29.1345	28.6061	31.6958
	LR	0.5620	0.2118	32.7513	31.2775	36.3388
	hyb	0.7597	0.5128	27.3926	27.2618	29.4406
DE	RF	0.6995	0.2377	10.7962	10.1582	10.9850
	BT	0.6841	0.2060	10.8842	10.6923	11.0267
	SVM	0.6299	0.0996	10.7696	10.4423	10.9545
	LR	0.6642	0.1659	10.8537	10.8572	10.9956
	hyb	0.6970	0.2325	9.9488	9.6865	10.0843
ES	RF	0.8087	0.5806	19.6511	17.9141	20.5422
	BT	0.8106	0.5844	17.5314	16.7036	18.2038
	SVM	0.7808	0.5269	18.1987	17.1226	18.9106
	LR	0.7906	0.5456	19.8148	18.3517	20.6706
	hyb	0.8108	0.5848	17.1232	16.2498	17.7346
FI	RF	0.6200	0.3290	29.8506	24.3231	36.3198
	BT	0.5735	0.2686	27.7375	22.8330	33.4742
	SVM	0.6255	0.3365	31.0392	25.1932	38.0917
	LR	0.5443	0.2330	31.8015	25.7889	39.3324
	hyb	0.6187	0.3273	28.5706	23.3520	34.6819
FR	RF	0.7738	0.5251	17.1205	15.8591	17.8289
	BT	0.7649	0.5089	15.8921	15.2586	16.4596
	SVM	0.7486	0.4796	19.3762	18.1085	20.2781
	LR	0.7829	0.5419	18.4691	17.1938	19.2378
	hyb	0.7719	0.5216	16.5098	15.6148	17.1457
IE	RF	0.5377	0.2598	40.1111	40.3074	53.9424
	BT	0.5456	0.2688	40.3111	41.7833	53.1313
	SVM	0.5428	0.2656	40.1513	41.2170	51.0510
	LR	0.5601	0.2854	38.5761	39.1479	59.9916
	hyb	0.5554	0.2800	39.6847	40.8462	51.3717

Country	ML	R	R^2	MAAPE	sMAPE	MAPEm
IT	RF	0.8797	0.7121	15.1892	14.7622	15.6488
	BT	0.8676	0.6852	15.7400	15.8513	16.1693
	SVM	0.8280	0.5996	17.5177	16.7230	18.3069
	LR	0.8577	0.6634	15.6623	15.3684	16.1714
	hyb	0.8734	0.6981	15.3097	15.0429	15.8176
LV	RF	0.8557	0.7286	48.9612	38.3661	96.2517
	BT	0.8496	0.7180	47.1245	37.2827	89.9710
	SVM	0.8763	0.7648	45.5753	35.8758	83.6064
	LR	0.8618	0.7392	48.0926	37.6909	96.6762
	hyb	0.8729	0.7588	46.4150	36.6295	87.1010
NO	RF	0.7127	0.4996	15.1716	14.4769	15.6007
	BT	0.7147	0.5025	14.7759	14.7968	15.0688
	SVM	0.7459	0.5489	14.6080	14.0406	14.9400
	LR	0.7801	0.6020	13.4537	12.8217	13.7872
	hyb	0.7479	0.5519	14.1211	13.8940	14.3901
PL	RF	0.7734	0.5405	24.4593	21.4467	26.6014
	BT	0.7614	0.5195	23.5249	20.7941	25.7269
	SVM	0.7444	0.4902	26.5439	23.7950	28.5871
	LR	0.7909	0.5719	24.4908	21.3049	26.7431
	hyb	0.7675	0.5301	24.0971	21.4187	26.0766
PT	RF	0.5415	0.2486	59.4413	46.8780	102.3002
	BT	0.5304	0.2359	57.1561	45.7869	94.0100
	SVM	0.6024	0.3227	56.0444	44.2971	90.6255
	LR	0.5888	0.3054	61.7878	49.9583	100.5018
	hyb	0.5730	0.2860	57.0015	45.3249	92.2630
RO	RF	0.6772	0.4264	23.5524	22.0246	24.7506
	BT	0.6779	0.4274	21.2217	20.7150	22.1505
	SVM	0.7564	0.5467	18.6972	18.4924	19.305
	LR	0.8039	0.6252	18.6243	17.7030	19.2287
	hyb	0.7285	0.5028	19.7350	19.3855	20.4253
SI	RF	0.5935	0.3185	24.6641	23.2484	26.6546
	BT	0.5546	0.2715	24.5130	24.0972	26.3103
	SVM	0.6714	0.4221	21.6664	21.2112	22.9135
	LR	0.6963	0.4580	26.3027	23.4225	28.9903
	hyb	0.6439	0.3841	22.7443	22.2739	24.1593
SI	RF	0.6012	0.3463	21.3937	21.4842	22.3222
	BT	0.5436	0.2789	22.2648	23.2707	23.2363
	SVM	0.7013	0.4799	19.6059	20.6566	20.319
	LR	0.7419	0.5398	20.3166	20.8063	21.0133
	hyb	0.6363	0.3908	20.6274	21.6530	21.4219
UK	RF	0.5897	0.4932	31.2177	28.4687	35.3760
	BT	0.5589	0.4971	30.1727	28.0854	33.9500
	SVM	0.5173	0.3644	32.3600	29.4185	39.1143
	LR	0.3668	0.2780	68.3851	69.9931	139.3174
	hyb	0.5685	-1.0927	30.4211	28.0844	34.5689

C Hydropower generation projections

Table 12: Difference in the annual average hydropower generation: comparison between 2016 [MW] and projections [%] for 2030 under RCP 4.5.

Country	2016[MW]	A45[%]	B45[%]	C45 [%]	D45[%]	E45[%]	F45 [%]	G45[%]	J45[%]	L45[%]	H45[%]	I45[%]
AT	3213.30	-7.05	-8.18	-9.19	-6.77	-6.86	-8.36	-6.43	-4.13	-3.49	-5.22	-6.65
BE	9.91	-23.25	-26.14	-24.70	-28.70	-27.69	-25.57	-21.29	-22.82	-23.92	-27.34	-26.35
BG	206.07	-2.04	-1.01	-0.87	-1.35	-1.72	-0.53	-0.08	-2.37	-1.44	-2.52	-1.21
CH	67.91	2.55	1.46	2.69	1.33	3.32	2.24	2.59	3.29	4.03	3.85	2.81
DE	1710.65	-2.20	-2.04	-1.93	-2.96	-2.37	-2.81	-2.07	-2.22	-2.67	-2.41	-2.92
ES	1021.11	-4.91	-4.28	-4.45	-4.59	-3.98	-2.18	-0.89	-4.11	-4.82	-3.94	-4.26
FI	1640.83	-4.43	-5.67	-4.63	-4.84	-5.62	-5.18	-5.84	-5.03	-5.28	-6.05	-5.95
FR	4799.32	-7.17	-7.29	-4.40	-7.71	-3.28	-1.42	-3.25	-1.00	-5.80	-7.76	-6.04
HU	11.28	-6.60	-5.88	-5.83	-5.73	-5.36	-5.15	-5.78	-6.52	-5.53	-6.56	-6.50
IE	76.00	-0.06	4.00	4.41	-0.15	-1.67	-2.43	-2.48	-0.27	1.88	1.91	1.29
IT	3536.11	1.53	1.76	2.16	2.88	3.51	2.78	3.32	2.21	2.91	2.82	2.52
LT	41.11	1.74	1.20	0.83	0.93	1.44	1.73	0.54	-0.13	0.08	0.17	-0.30
LV	291.45	21.70	21.73	19.79	20.02	21.48	23.02	21.27	16.72	21.99	20.10	19.26
NO	1285.76	-4.43	-5.94	-3.96	-6.01	-4.66	-5.35	-5.98	-2.98	-6.43	-4.19	-5.25
PL	178.55	-4.40	-5.52	-6.13	-6.52	-6.44	-7.07	-7.57	-6.34	-7.47	-6.47	-7.13
PT	1078.98	-20.20	-19.76	-19.77	-21.66	-24.31	-20.31	-20.20	-23.62	-22.55	-22.39	-22.03
RO	1307.58	-4.62	-2.74	-3.02	-4.05	-2.27	-2.52	-0.19	-4.98	-0.48	-2.87	-2.29
SI	496.22	-6.67	-6.33	-6.53	-7.73	-6.78	-7.16	-4.39	-6.71	-7.28	-7.02	-6.50
SK	458.64	-6.23	-4.99	-7.51	-6.74	-6.07	-5.88	-6.06	-8.20	-6.35	-6.96	-6.23
UK	384.99	4.30	7.42	7.29	4.47	4.95	0.79	1.89	4.82	5.37	4.79	5.69

Table 13: Difference in the annual average hydropower generation: comparison between 2016 [MW] and projections [%] for 2050 under RCP 4.5.

Country	2016 [MW]	A45[%]	B45 [%]	C45[%]	D45[%]	E45[%]	F45[%]	G45[%]	J45[%]	L45[%]	H45[%]	I45[%]
AT	3213.30	-7.11	-6.61	-9.09	-6.36	-6.30	-8.17	-5.37	-4.97	-3.64	-5.30	-6.62
BE	9.91	-22.43	-26.49	-25.11	-29.73	-27.82	-24.87	-20.51	-23.19	-24.60	-27.13	-27.06
BG	206.07	-2.28	-1.46	-1.11	-1.98	-2.25	-1.53	-1.07	-2.78	-1.98	-3.15	-1.66
CH	67.91	2.61	1.92	3.33	1.21	3.86	3.24	4.35	3.59	4.89	3.45	2.48
DE	1710.65	-2.32	-2.57	-2.72	-3.25	-2.76	-2.52	-2.18	-2.52	-2.37	-2.91	-3.32
ES	1021.11	-5.67	-4.99	-5.42	-5.94	-5.11	-2.42	-1.40	-4.25	-6.02	-4.66	-4.88
FI	1640.83	-4.24	-5.54	-4.51	-4.74	-5.26	-5.25	-5.43	-4.84	-5.13	-6.26	-5.74
FR	4799.32	-7.30	-8.57	-6.34	-9.41	-4.95	-1.34	-4.42	-2.08	-7.38	-9.83	-8.40
HU	11.28	-7.00	-5.98	-6.59	-6.14	-5.43	-5.99	-5.98	-7.11	-5.85	-6.70	-6.59
IE	76.00	0.42	2.78	2.37	-0.58	-2.26	-2.57	-1.95	-0.70	2.69	2.95	2.37
IT	3536.11	1.10	1.56	1.55	2.52	3.43	2.60	2.86	1.84	2.71	2.72	2.57
LT	41.11	1.21	1.69	0.22	-0.57	0.79	1.14	-0.37	-1.13	0.09	-1.21	-1.33
LV	291.45	20.66	20.47	19.08	17.60	20.49	23.15	21.38	17.46	20.98	18.45	17.34
NO	1285.76	-4.53	-5.55	-3.59	-6.28	-4.55	-4.91	-4.97	-2.56	-5.99	-4.16	-5.15
PL	178.55	-5.20	-5.60	-6.22	-6.64	-6.54	-6.95	-7.22	-5.69	-6.99	-7.10	-7.46
PT	1078.98	-20.75	-20.37	-20.91	-23.58	-27.44	-20.13	-19.97	-24.95	-24.43	-23.75	-23.41
RO	1307.58	-4.40	-3.12	-3.12	-3.52	-1.70	-2.81	-0.40	-5.15	-1.09	-3.45	-3.20
SI	496.22	-6.59	-6.94	-6.65	-6.88	-6.94	-5.99	-3.37	-6.81	-7.27	-7.46	-6.99
SK	458.64	-5.93	-5.65	-7.94	-8.30	-6.70	-6.69	-5.43	-8.29	-6.81	-7.71	-6.87
UK	384.99	5.08	6.61	6.67	4.34	4.47	0.88	2.84	4.67	5.58	5.55	5.66

Table 14: Difference in the annual average hydropower generation: comparison between 2016 [MW] and projections [%] for 2030 under RCP 8.5.

Country	2016[MW]	A85[%]	B85[%]	C85 [%]	D85[%]	E85[%]	F85[%]	G85[%]	J85[%]	L85[%]	H85[%]	I85 [%]
AT	3213.30	-9.06	-6.06	-9.07	-6.74	-1.97	-5.19	-7.17	-10.66	-7.74	-6.27	-5.21
BE	9.91	-24.34	-27.78	-25.24	-22.69	-23.31	-22.94	-25.31	-29.30	-27.37	-25.27	-26.92
BG	206.07	-2.61	-2.15	-1.84	-1.72	-3.57	-1.24	-1.07	-0.88	-3.04	-1.60	-1.37
CH	67.91	3.35	1.84	1.26	3.30	2.08	3.96	3.84	2.58	4.17	3.83	3.82
DE	1710.65	-2.27	-1.67	-2.35	-2.85	-2.49	-1.69	-2.00	-2.86	-3.17	-2.79	-2.67
ES	1021.11	-4.24	-3.33	-3.88	-4.59	-4.24	-6.35	-5.56	-4.71	-4.31	-6.07	-5.42
FI	1640.83	-5.54	-4.90	-4.57	-4.97	-5.21	-4.97	-6.34	-5.33	-6.44	-5.46	-5.85
FR	4799.32	-7.03	-7.31	-2.65	-7.61	-3.31	-6.34	-7.95	-9.37	-8.74	-9.37	-12.02
HU	11.28	-6.29	-6.08	-5.89	-5.97	-5.95	-5.45	-5.37	-5.67	-6.35	-6.31	-6.42
IE	76.00	4.22	1.45	0.70	4.13	2.23	1.45	0.55	1.78	4.37	-0.65	2.02
IT	3536.11	1.16	2.29	2.52	1.91	1.57	2.61	1.91	2.19	2.56	2.02	1.97
LT	41.11	-0.29	1.83	0.53	-0.75	1.13	2.77	2.10	-1.25	-0.42	0.53	-0.02
LV	291.45	19.13	21.45	19.02	16.01	18.66	23.35	22.19	16.38	17.28	18.30	18.94
NO	1285.76	-5.50	-4.12	-4.10	-2.53	-5.85	-4.12	-6.57	-4.92	-4.03	-4.00	-4.78
PL	178.55	-7.76	-4.47	-7.32	-7.63	-6.76	-4.16	-3.98	-8.12	-7.69	-6.60	-6.52
PT	1078.98	-25.72	-23.00	-23.24	-26.14	-22.63	-27.90	-26.61	-25.44	-23.38	-25.70	-24.97
RO	1307.58	-6.34	-2.74	-2.56	-3.14	-3.47	-1.77	-1.40	-5.14	-3.41	-4.00	-3.50
SI	496.22	-7.27	-5.85	-6.55	-6.78	-6.69	-5.90	-5.27	-7.18	-5.24	-7.64	-7.10
SK	458.64	-7.78	-6.02	-7.88	-8.27	-7.86	-5.89	-4.15	-8.11	-8.76	-7.71	-6.86
UK	384.99	7.59	5.91	5.77	6.79	5.97	4.05	4.56	5.95	5.64	5.20	5.78

Table 15: Difference in the annual average hydropower generation: comparison between 2016 [MW] and projections [%] for 2050 under RCP 8.5.

Country	2016[MW]	A85[%]	B85[%]	C85[%]	D85[%]	E85[%]	F85[%]	G85[%]	J85[%]	L85[%]	H85[%]	I85[%]
AT	3213.30	-8.38	-5.83	-8.00	-7.18	-1.15	-5.31	-5.73	-9.55	-7.32	-7.85	-5.44
BE	9.91	-22.50	-27.77	-25.16	-24.35	-22.27	-21.58	-25.55	-27.55	-26.61	-24.90	-26.51
BG	206.07	-2.82	-2.88	-2.68	-1.93	-4.50	-2.30	-2.58	-2.66	-3.48	-2.47	-2.56
CH	67.91	3.49	3.00	3.36	2.62	4.22	4.56	5.02	3.03	4.25	4.65	3.94
DE	1710.65	-2.24	-2.28	-3.35	-3.05	-2.84	-1.91	-2.39	-3.28	-2.70	-3.10	-2.78
ES	1021.11	-6.46	-4.46	-4.91	-5.75	-4.97	-7.56	-6.46	-5.97	-5.24	-7.81	-7.30
FI	1640.83	-5.67	-4.60	-4.31	-5.34	-5.43	-4.58	-5.94	-5.12	-6.40	-5.40	-5.57
FR	4799.32	-7.40	-9.31	-5.01	-9.18	-3.58	-8.08	-10.72	-10.52	-9.68	-11.82	-14.89
HU	11.28	-6.36	-6.00	-6.35	-5.92	-6.78	-6.03	-6.63	-6.74	-6.22	-6.46	-6.58
IE	76.00	5.67	1.75	1.21	3.98	1.18	2.16	1.71	1.72	4.59	0.76	2.62
IT	3536.11	0.77	1.76	1.68	1.33	1.23	1.91	1.29	1.47	2.46	1.49	1.40
LT	41.11	-0.97	0.93	-0.71	-2.39	0.28	1.67	0.88	-3.17	-0.54	-1.38	-1.21
LV	291.45	16.43	20.15	16.91	13.44	20.50	21.89	21.22	13.30	15.65	16.72	17.60
NO	1285.76	-4.95	-4.02	-4.68	-2.07	-5.96	-3.63	-5.80	-4.83	-3.91	-3.55	-4.69
PL	178.55	-7.22	-4.68	-7.12	-8.43	-6.43	-3.69	-4.08	-8.08	-6.98	-7.46	-7.76
PT	1078.98	-29.06	-23.80	-25.70	-27.68	-24.75	-27.52	-25.04	-25.51	-24.05	-28.86	-28.32
RO	1307.58	-5.36	-2.88	-2.18	-2.94	-2.40	-1.48	-1.98	-4.99	-3.17	-4.47	-4.39
SI	496.22	-7.19	-7.01	-6.69	-6.20	-5.89	-5.52	-5.10	-6.87	-4.84	-8.02	-7.16
SK	458.64	-7.56	-6.04	-7.99	-8.85	-7.60	-6.20	-4.12	-8.23	-8.14	-8.47	-7.68
UK	384.99	8.33	5.58	5.80	7.79	6.97	4.42	4.53	6.04	5.82	6.13	6.60

References

[1] International hydropower association. Hydropower status report: sector trends and insights, [online] Available at: https://www.hydropower.org/status2019 [accessed Dec. 2019].

[2] B. Stoll, J. Andrade, S. Cohen, G. Brinkman, C. Brancucci Martinez-Anido, Hydropower modeling challenges, Tech. Rep. WFGX. 1040, National Renewable Energy Laboratory, www.nrel.gov/publications (2017).

[3] B. Hamududu, A. Killingtveit, Assessing climate change impacts on global hydropower, Energies 5 (2012) 305–322.

[4] N. A. Treiber, J. Heinermann, O. Kramer, Computational Sustainability, Studies in Computational Intelligence, Vol. 645, Springer International Publishing Switzerland, 2016, Ch. Wind Power Prediction with Machine Learning.

[5] C. Voyant, G. Notton, S. Kalogirou, M.-L. Nivet, C. Paoli, F. Motte, A. Fouilloy, Machine learning methods for solar radiation forecasting: A review, Renew. Energ. 105 (2017) 569–582.

[6] F. Kratzert, D. Klotz, C. Brenner, K. Schulz, M. Herrnegger, Rainfall-runoff modelling using Long Short-Term Memory (LSTM) networks, Hydrol. Earth Syst. Sci. 22 (2018) 6005–6022.

[7] P. Drobinski, Wind and solar renewable energy potential resources estimation, Encyclopedia of Life Support Systems (EOLSS) (2012).

[8] L. Gaudard, F. Romerio, The future of hydropower in Europe: Interconnting climate, markets and policies, Envir. Sci. Policy 37 (2014) 172–181.

[9] B. Schaefli, Projecting hydropower production under future climates: a guide for decision-makers and modelers to interpret and design climate change impact assessments, WIREs Water 2 (2015) 271–289.

[10] M. D. Felice, L. Dubus, E. Suckling, A. Troccoli, The impact of the North Atlantic Oscillation on European hydropower generation, submitted to Appl. Energ.Preprint available at: https://eartharxiv.org/8sntx/.

[11] CLIM2POWER web service, [online] Available at: https://clim2power.com [accessed Dec. 2019].

[12] S. G. Simoes, F. Amorim, G. Siggini, V. Sessa, Y.-M. Saint-Drenan, S. Carvalho, H. Mraihi, E. Assoumou, Climate proofing the renewable electricity deployment in Europe - introducing climate variability in large energy systems models, (submitted).

[13] O. J. Guerra, D. A. Tejada, G. V. Reklaitis, Climate change impacts and adaptation strategies for a hydro-dominated power system via stochastic optimization, Appl. Energ. 233-234 (2019) 584–598.

[14] A. F. P. de Lucena, R. Schaeffer, A. Szklo, Least-cost adaptation options for global climate change impacts on the brazilian electric power system, Glob. Environ. Chang. 20 (2010) 342–350.

[15] X. Liu, Q. Tang, N. Voisin, H. Cui, Projected impacts of climate change on hydropower potential in china, Hydrol. Earth Syst. Sci. 20 (2016) 3343–3359.

[16] B. J. R. Spalding-Fecher, H. Winkler, Climate change and hydropower in the southern african power pool and zambezi river basin: system-wide impacts and policy implications, Energ. Policy 13 (2017) 84–97.

[17] B. Boehlert, K. M. Strzepek, Y. Gebretsadik, R. Swanson, A. McCluskey, J. E. Neumann, J. McFarland, J. Martinich, Climate change impacts and greenhouse gas mitigation effects on U.S. hydropower generation, Appl. Energ. 183 (2016) 1511–1519.

[18] German meteorological service (DWD – deutscher wetterdienst), esgf.dwd.de/projects/esgf-dwd/ [accessed Jan. 2019].

[19] European Network of Transmission System Operator for Electricity, [online] https://www.entsoe.eu/ [accessed Dec. 2019].

[20] F. Giorgi, C. Jones, G. R. Asrar, Addressing climate information needs at the regional level: the cordex framework, Bull. - World Meteorol. Organ. 58 (2009) 175–183.

[21] D. Jacob, et al., Euro-cordex: new high-resolution climate change projections for European impact research, Reg. Environ. Chang. 14 (2014) 563–578.

[22] R. M. et al., Towards new scenarios for analysis of emissions, climate change, impacts and response strategies, Tech. rep., Technical Summary. Intergovernmental Panel on Climate Change, Geneva, p.25 (2008).

[23] E. Hawkins, T. M. Osborne, C. K. Ho, A. J. Challinorc, Calibration and bias correction of climate projections for crop modelling: An idealised case study over europe, Agr. Forest Meteorol 170 (2013) 19–31.

[24] R. Knutti, J. Sedláček, Robustness and uncertainties in the new cmip5 climate model projections, Nat. Clim. Chang. 3 (2013) 369–373.

[25] A. F. Prein, A. Gobiet, Impacts of uncertainties in European gridded precipitation observations on regional climate analysis, Int. J. Climatol. 37 (2017) 305–327.

[26] T. Stocker, D. Qin, G.-K. Plattner, M. Tignor, S. Allen, J. Boschung, A. Nauels, Y. Xia, V. Bex, P. M. Midgley, Climate Change 2013: The Physical Science Basis, Contribution of Working Group I to the Fifth Assessment Report of the Intergovernmental Panel on Climate Change, Cambridge University Press: Cambridge, UK and New York, USA, 2013.

[27] T. Hastie, R. Tibshirani, J. Friedman, The Elements of Statistical Learning, Springer-Verlag New York, 2009.

[28] A. J. Smola, B. Schölkopf, A tutorial on support vector regression, Stat. Comp. 14 (2004) 199–222.

[29] J. H. Friedman, Greedy function approximation: A gradient boosting machine, The Annals of Statistics 29 (2001) 1189–1232.

[30] L. Breiman, Random forests, Mach. Learn. 45 (2001) 5–32.

[31] MATLAB and Statistics and Machine Learning Toolbox release 2018b, the MathWorks, Inc., Natick, Massachusetts, United States.

[32] H. Drucker, C. J. Burges, L. Kaufman, A. Smola, V. Vapnik, Support vector regression machines, Adv. Neur. In. (1997) 155–161.

[33] Y. Gala, A. Fernández, J. Díaz, J. R. Dorronsoro, Hybrid machine learning forecasting of solar radiation values, Neurocomputing 176 (2016) 48–59.

[34] K. Pearson, Notes on regression and inheritance in the case of two parents, in: Proceedings of the Royal Society of London, Vol. 58, 1895, p. 240–242.

[35] S. Kim, H. Kim, A new metric of absolute percetage error for intermittent demand forecasts, Int. J. Forecasting 32 (2016) 669–679.

[36] S. Makridakis, Accuracy measures: theoretical and practical concerns, Int. J. Forecasting 9 (1993) 527–529.

[37] Energias de portugal (edp, [online] Available at: https://a-nossa-energia.edp.pt~[accessedDec.2018],.